Lithos 323 (2018) 4–23

Contents lists available at ScienceDirect

Lithos

journal homepage: www.elsevier.com/locate/lithos

From mantle peridotites to hybrid troctolites: Textural and chemical evolution during melt-rock interaction history (Mt. Maggiore, Corsica, France)

Valentin Basch [a,*], Elisabetta Rampone [a], Laura Crispini [a], Carlotta Ferrando [b], Benoit Ildefonse [b], Marguerite Godard [b]

[a] DISTAV, University of Genova, Corso Europa 26, I-16132 Genova, Italy
[b] Géosciences Montpellier, University of Montpellier, CNRS, Montpellier, France

ARTICLE INFO

Article history:
Received 19 October 2017
Accepted 21 February 2018
Available online 27 February 2018

Keywords:
Alpine ophiolites
Melt-rock interaction
Reactive porous flow
Melt impregnation
Olivine texture
Olivine trace elements

ABSTRACT

Recent studies investigate the replacive formation of hybrid troctolites from mantle peridotites after multiple stages of melt-rock reaction. However, these studies are not conducted in a field-controlled geological setting displaying the clear evolution from the protolith to the end-product of the reactions. The Mt. Maggiore peridotitic body exposes a clear evolution from spinel lherzolite to plagioclase-bearing lithotypes (plagioclase peridotites, olivine-rich troctolites and troctolites) during two continuous episodes of melt-rock interaction. In the spinel facies, the reactive percolation of a LREE-depleted melt leads to the dissolution of mantle pyroxenes and the growth of olivine crystals, forming replacive spinel dunites. The progressive evolution from spinel lherzolite to harzburgite to replacive dunite is accompanied by a change of olivine Crystallographic Preferred Orientation (CPO), from axial-[100] in the lherzolite to axial-[010] olivine CPO in the dunites, indicative of deformation in presence of melt. The initial percolating melt composition is consistent with single melt increments after 6% partial melting of a depleted mantle source. Reactive melt percolation leads to a progressive enrichment in the melt M-HREE absolute concentrations, while preserving its LREE depletion, consistent with the enriched analyzed HREE composition of olivine in the spinel dunite.

In the shallower plagioclase facies, the melts modified by reactive melt percolation impregnate the spinel-facies lithotypes, leading to the dissolution of olivine and crystallization of plagioclase and orthopyroxene in the peridotites. This impregnation stage is also observed in the spinel dunites, forming hybrid olivine-rich troctolites and troctolites. The dissolution-precipitation reactions forming hybrid troctolites cause a progressive textural evolution of the olivine matrix, with the disruption of deformed coarse grains into undeformed small rounded grains. This textural evolution is not accompanied by clear changes in the olivine CPO, indicating low instantaneous melt/rock ratios during the impregnation process. Olivine, plagioclase and clinopyroxene REE compositions analyzed in troctolite fit a process of impregnation with a progressive closure of the porosity (at decreasing melt mass), leading to the crystallization of trapped melt and REE enrichments during the last crystallization increments.

1. Introduction

Many studies have highlighted the importance of melt-rock interactions in developing structural and geochemical heterogeneities in peridotites at different mantle depths (e.g., Collier and Kelemen, 2010; Dijkstra et al., 2001, 2003; Dygert et al., 2016; Higgie and Tommasi, 2012, 2014; Lissenberg and Dick, 2008; Paquet et al., 2016; Saper and Liang, 2014; Soustelle et al., 2009, 2010, 2014; Tursack and Liang, 2012). Specifically, melt-rock reactions have been invoked as important rock-forming processes acting in the upwelling mantle in extensional settings. In such geodynamic environments, replacive spinel harzburgites and dunites have been inferred as the product of open-system reactive melt percolation, driven by pyroxene dissolution and olivine crystallization at deep (spinel-facies) mantle levels (e.g., Dick et al., 2008, 2010; Dygert et al., 2016; Kelemen et al., 1995a, b, 2000, 2007; Lambart et al., 2009; Liang et al., 2011; Piccardo et al., 2007; Pirard et al., 2013; Rampone et al., 2008; Rampone and Borghini, 2008), whereas plagioclase-rich peridotites, ubiquitously found in ophiolitic and oceanic settings, are widely thought to result from melt impregnation at shallower (plagioclase-facies) mantle depths (e.g., Borghini et al., 2007; Dijkstra et al., 2001, 2003; Rampone and Borghini, 2008; Saper and Liang, 2014; Tursack and Liang, 2012).

* Corresponding author at: Dipartimento di Scienze della Terra, dell'Ambiente e della Vita (DISTAV), Università degli Studi di Genova, Corso Europa 26, I-16132 Genova, Italy.
E-mail address: valentin.basch@gmail.com (V. Basch).

https://doi.org/10.1016/j.lithos.2018.02.025
0024-4937/

Melt-rock interactions have also been increasingly invoked as key processes in the formation and compositional evolution of the oceanic crust, from several lines of evidence: (1) the study of chemical zoning and melt inclusions in lava phenocrysts (Coumans et al., 2016; Laubier et al., 2014), (2) peculiar compositional trends observed in mid-ocean ridge basalts (MORBs), not consistent with a process of pure fractional crystallization (Collier and Kelemen, 2010; Paquet et al., 2016; Van den Bleeken et al., 2011), (3) olivine-rich troctolites found enclosed in the lowermost oceanic crust, thought to represent the "hybrid" reactive product of the interaction between dunites from the crust-mantle boundary and percolating MORB melts, dissolving olivine and crystallizing interstitial plagioclase and clinopyroxene (Lissenberg and Dick, 2008; Suhr et al., 2008; Drouin et al., 2009, 2010; Renna and Tribuzio, 2011; Sanfilippo and Tribuzio, 2012; Higgie and Tommasi, 2012; Sanfilippo et al., 2013, 2014, 2015, 2016; Rampone et al., 2016; Renna et al., 2016). These latter studies have thus inferred the possible incorporation of mantle slivers into the lower oceanic crust at slow-spreading ridges through multiple melt-rock interaction episodes leading to the replacive formation of dunites, olivine-rich troctolites and troctolites from mantle peridotites. However, the mantle origin of the dunitic matrix and the resulting hybrid origin of troctolites (i.e., by dunite melt impregnation rather than by fractional crystallization of a primitive melt) is difficult to demonstrate without documenting the evolution from mantle peridotite protolith to the hybrid end-product.

The Alpine-Apennine ophiolites are predominantly constituted by mantle peridotites and represent analogues of the oceanic lithosphere formed at ocean/continent transition and slow- to ultra-slow spreading settings (Borghini et al., 2007; Manatschal and Müntener, 2009; Marroni et al., 1998; Müntener et al., 2004; Müntener and Piccardo, 2003; Piccardo et al., 2004; Rampone et al., 1997, 2004, 2008; Rampone and Piccardo, 2000; Sanfilippo and Tribuzio, 2011; Tribuzio et al., 2016). Previous studies have documented that many Alpine-Apennine peridotites record various stages of melt-rock interaction, which occurred at different lithospheric levels during the extensional mantle exhumation (e.g. Piccardo and Guarnieri, 2010; Rampone and Borghini, 2008).

The Mt. Maggiore (Alpine Corsica) peridotitic body displays lithological variations clearly related to two episodes of melt-rock interaction: a first reactive melt percolation event at spinel-facies, leading to the replacive formation of harzburgites and dunites, followed by melt impregnation of the spinel peridotites and dunites at plagioclase-facies, crystallizing plagioclase ± orthopyroxene, and dissolving olivine (Jackson and Ohnenstetter, 1981; Müntener and Piccardo, 2003; Piccardo and Guarnieri, 2010; Rampone et al., 1997, 2008). In the field, the primary association between spinel- and plagioclase- peridotites, dunites, and olivine-rich troctolites is preserved, and the replacive formation of plagioclase peridotites and troctolites from the spinel-facies lithotypes during the melt impregnation stage is therefore clearly recognizable. The Mt. Maggiore peridotitic body is thus an ideal case study to investigate the structural and geochemical evolution of a mantle peridotite protolith during the multiple melt-rock interaction stages leading to the replacive formation of hybrid troctolites.

In this paper, we present new field mapping, coupled with Electron Backscatter Diffraction (EBSD) measurements, and mineral major and trace elements analyses (by Electron Probe Micro-Analyses (EPMA) and Laser Ablation-Inductively Coupled Plasma-Mass Spectrometry (LA-ICP-MS), respectively) of Mt. Maggiore spinel and plagioclase peridotites, spinel dunites, and troctolites, which aim at documenting and discussing the textural and mineral chemical changes during formation of hybrid troctolites. We focus specifically on combined textural observations (EBSD mapping) and trace element geochemistry of olivine. Olivine is the major constituent in peridotites and troctolites, and is extensively involved in the melt-rock reactions described in the oceanic lithosphere. Although the behaviour of many trace elements in olivine is still poorly understood, recent studies outlined the potential of olivine minor and trace elements in the investigation of mantle processes, from melting to melt-rock interactions (e.g., De Hoog et al., 2010; D'Errico et al., 2016; Drouin et al., 2009; Foley et al., 2013; Lissenberg et al., 2013; Rampone et al., 2016; Sanfilippo et al., 2014).

Here we show that the trace element composition of olivine, coupled to EBSD analyses, on a field-controlled sample set, constitute a powerful approach to investigate melt-rock reaction processes leading to the origin of hybrid troctolites. Major outcomes of this work are the demonstrated and quantified textural evolution of the olivine matrix during the replacive formation of hybrid troctolites, and the evidence for microstructural and geochemical inheritance of olivine in the troctolites from both dunite-forming and troctolite-forming melt-rock interaction stages.

2. Structural and petrologic background

The Corsican mafic-ultramafic bodies are part of the Alpine-Apennine ophiolites, thought to represent the lithosphere remnants of the narrow Jurassic Ligurian Tethys basin (400–500 km) opened by passive lithosphere extension leading to slow- to ultra-slow spreading oceanization (Manatschal and Müntener, 2009; Rampone and Piccardo, 2000). The Mt. Maggiore peridotitic massif has been interpreted as the deepest part of the reconstructed "Schistes Lustrés" ophiolitic sequence, exposed in the eastern Alpine Corsica (Fig. 1) (Jackson and Ohnenstetter, 1981). Although it lacks any crustal cover, it preserves clear field relationships between the mantle peridotites and associated pyroxenite and gabbroic lithotypes. Previous studies showed that the peridotitic body records a multi-stage lithospheric exhumation history, through various episodes of melt-rock interaction from deep (spinel-facies) to shallower levels (plagioclase-facies) (Müntener and Piccardo, 2003; Piccardo and Guarnieri, 2010; Rampone et al., 1997, 2008).

A first event of olivine-saturated reactive melt percolation leads to the dissolution of mantle clinopyroxene and orthopyroxene, and crystallization of olivine at spinel facies conditions. This melt-rock interaction is recorded in the spinel lherzolites and harzburgites by the development of olivine embayments partly replacing mantle orthopyroxene and clinopyroxene. Extensive reactive melt percolation is observed with the replacive formation of spinel dunite pods and the partial to complete dissolution of pyroxenite layers primarily associated with the spinel peridotites. In the clinopyroxene-poor spinel lherzolites and harzburgites, the trace element compositions of clinopyroxenes are relatively homogeneous and LREE depleted, consistent with residual mantle after low-degrees (5–8%) of fractional melting (Rampone et al., 1997, 2008).

In the field, the Mt. Maggiore spinel peridotites grade to plagioclase-bearing peridotites showing microstructural characteristics indicative of a plagioclase- (±opx) crystallizing, olivine-dissolving melt impregnation (Müntener and Piccardo, 2003; Piccardo and Guarnieri, 2010; Rampone et al., 1997, 2008). Highly impregnated plagioclase peridotites often display plagioclase-rich gabbronoritic veinlets, crystallized after segregation of the percolating melts. Rock-forming minerals in the gabbronoritic veinlets also show LREE depleted patterns, indicating the depleted signature of the impregnating melts, which thus do not correspond to an aggregated MORB (Rampone et al., 2008).

Together, the reported melt-rock interaction processes suggest the open-system reactive percolation of an olivine-saturated depleted melt at spinel facies levels followed by impregnation of the peridotites by migrating melts at shallower, colder lithospheric depths. Rampone et al. (2008) described the progressive modification of the percolating melt composition during the pyroxene-dissolving, olivine-crystallizing reactive melt percolation. They inferred that melt-rock interaction occurring at spinel-facies led to a progressive decrease in the olivine saturation and increase in pyroxene and plagioclase saturation. Together with a change in lithospheric depth during upwards melt percolation (from spinel-facies to plagioclase-facies), the compositional variations of the melt enabled an evolution in the type of melt-rock interaction from an olivine-crystallizing, pyroxene-dissolving reactive melt percolation at spinel-facies to a plagioclase ± orthopyroxene ± clinopyroxene

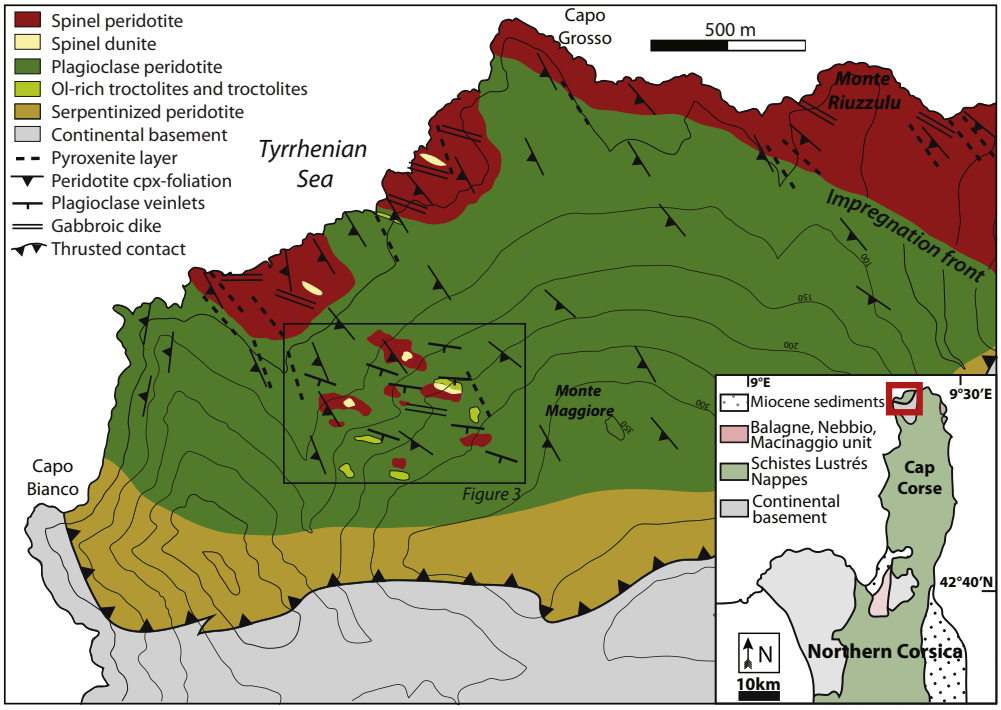

Fig. 1. Geological map of the lithological variations and associated structures of the Mt. Maggiore peridotites (Corsica). This structural map merges new data measured on the field with the data of Jackson and Ohnenstetter (1981). The black square represents the area studied into more detail, where the sampling has been done. A schematic sketch of the structures and field associations mapped in this area is shown in Fig. 3. The impregnation front marks the contact between the spinel-facies and plagioclase-facies lithotypes.

melt impregnation at plagioclase-facies. Both spinel and plagioclase peridotites were intruded by later gabbroic dykes, ranging from olivine gabbros to diorites, showing a clear MORB-type affinity (Piccardo and Guarnieri, 2010).

3. Geology of the studied area

We performed a detailed mapping of the Monte Maggiore peridotitic body and merged our lithological and structural data with the already published data of Jackson and Ohnenstetter (1981) in Fig. 1. The Mt. Maggiore peridotitic massif is mainly composed of granular spinel and plagioclase peridotites, showing in places a weak foliation with a preferential elongation of mantle pyroxenes (Fig. 1). The spinel peridotites show variations in modal compositions, ranging from olivine-poor lherzolites (60% olivine) to olivine-rich harzburgites (85% olivine) (Table 1). The mantle peridotites are primarily associated to decimetre-size sub-vertical pyroxenite layers, showing a constant NW-SE orientation. In places, these pyroxenite layers are partially dissolved. Similar sub-vertical NW-SE orientations are reported for the foliation observed in the spinel peridotites. In places, the spinel peridotites progressively

Table 1
Studied samples, modal compositions and mean textural parameters of the olivine matrix.

		Modal composition					Textural parameters				
Sample	Lithotype	Ol	Plg	Cpx	Opx	Sp	No grains	Grain area (mm^2)	Aspect ratio	PARIS factor	Shape factor
M15/7	Sp. lherzolite	58	0	11	25	6	63	3.81	1.64	177	2.46
M15/7B	Sp. lherzolite	62	0	13	23	2	44	8.04	1.64	209	2.64
M15/13	Sp. harzburgite	78	0	2	20	0	40	8.47	1.73	161	2.35
M15/15	Plag. lherzolite	74	0	10	15	1	42	9.71	1.67	90	1.82
M15/12B	Plag. harzburgite	65	8	8	18	1	40	7.44	1.69	159	2.29
M15/20A	Plag. harzburgite	58	17	1	24	0	28	7.35	1.67	214	2.65
M15/18A	Plag. harzburgite	50	25	1	24	0	33	6.82	1.52	133	2.04
M15/19	Plag. harzburgite	50	18	7	25	0	21	5.82	1.56	149	2.19
M15/19B	Plag. harzburgite	48	15	6	31	0	37	5.73	1.83	158	2.28
M15/3	Spinel dunite	97	0	0	0	3	12	38.8	1.71	179	2.49
M15/5	Spinel dunite	99	0	0	0	1	51	7.02	1.67	158	2.22
M15/14	Spinel dunite	99	0	0	0	1	24	19.08	1.85	143	2.25
M15/9	Ol-rich troctolite	85	15	0	0	0	37	10.35	1.59	154	2.24
M15/8A2	Ol-rich troctolite	82	17	0	0	1	39	11.56	1.76	132	2.07
M15/1	Ol-rich troctolite	80	20	0	0	0	55	7.00	1.71	105	1.89
M15/11	Ol-rich troctolite	78	20	0	0	2	51	7.24	1.63	111	1.92
M15/8A3[a]	Troctolite	75	14	10	0	1	41	9.14	1.43	125	1.92
M15/10A[b]	Troctolite	74	18	2	5	1	82	4.60	1.54	108	1.86
M15/8B	Troctolite	73	25	1	0	1	44	9.45	1.63	125	1.77
M15/8A	Troctolite	73	25	1	0	1	36	11.53	1.54	112	1.86
M15/6	Troctolite	71	23	1	0	5	32	11.99	1.71	110	1.91
M15/10B[b]	Troctolite	70	19	3	7	1	59	5.29	1.59	128	2.11

[a] Clinopyroxene-bearing troctolite.
[b] Sample at the contact between plagioclase peridotite and troctolite.

grade to metre-size spinel dunitic bodies, through a diffuse to sharp contact (Fig. 2a,b). The occurrence of aligned spinel trails within the dunite suggests the former presence of a pyroxenite layer, in which pyroxenes were completely dissolved (Fig. 2b), further evidences the replacive nature of the spinel dunites (Piccardo and Guarnieri, 2010).

The spinel peridotites grade to plagioclase-bearing peridotites, showing an enrichment in interstitial plagioclase and orthopyroxene. The most plagioclase-rich samples (up to 30% interstitial minerals) show a steeply dipping (50–70°S) modal layering of plagioclase enrichment, oriented ESE-WNW (Figs. 1, 3), and associated gabbronoritic veinlets (Fig. 2c). The plagioclase peridotites are associated to bodies of olivine-rich troctolites and troctolites, previously described as "cumulates" (Rampone et al., 1997; Müntener and Piccardo, 2003; Piccardo and Guarnieri, 2010). Based on new field observations, we infer that these troctolitic bodies correspond to the plagioclase-facies melt impregnation of the spinel dunites. At the impregnation front, i.e. the transition from preserved spinel-bearing lithotypes to impregnated plagioclase-bearing lithotypes, the spinel peridotite and associated dunite pods grade to replacive plagioclase peridotite and troctolitic bodies, respectively. These troctolitic bodies have variable modal compositions from 70 to 90% of granular olivine and up to 30% of interstitial plagioclase (Fig. 2d,e). The most impregnated samples show a ESE-WNW layering of plagioclase enrichment and formation of gabbronoritic veinlets, similar to what is observed in the plagioclase peridotite (Figs. 1, 3). All spinel- and plagioclase-bearing lithotypes and structures are crosscut by steeply dipping gabbroic dikes (60–80°S), trending E-W to ESE-WNW (Figs. 1, 3).

At the scale of the massif, zones that preserve the primary evolution of mantle peridotites and associated lithologies are separated by low-grade alteration zones rich in serpentine veins (reported as *Serpentine veinlets-bearing peridotite* in Fig. 3). These veinlets often show a common orientation and thus form bands of altered peridotites, surrounding lenses of fresh granular peridotites (Fig. 3). Based on the field occurrences and lithological associations, we selected an area preserved of extensive alteration, and bearing primary associations from spinel- to plagioclase-bearing lithotypes (Fig. 3) to perform detailed mapping (black box in Fig. 1) and sampling.

4. Sampling and analytical methods

In the selected area (Fig. 1), we collected samples along traverses showing primary associations of spinel peridotite and spinel dunite, grading to plagioclase peridotite, olivine-rich troctolite and troctolite. Table 1 reports the modal composition of 22 samples, namely 3 spinel peridotites, 3 spinel dunites, 6 plagioclase peridotites, 4 olivine-rich

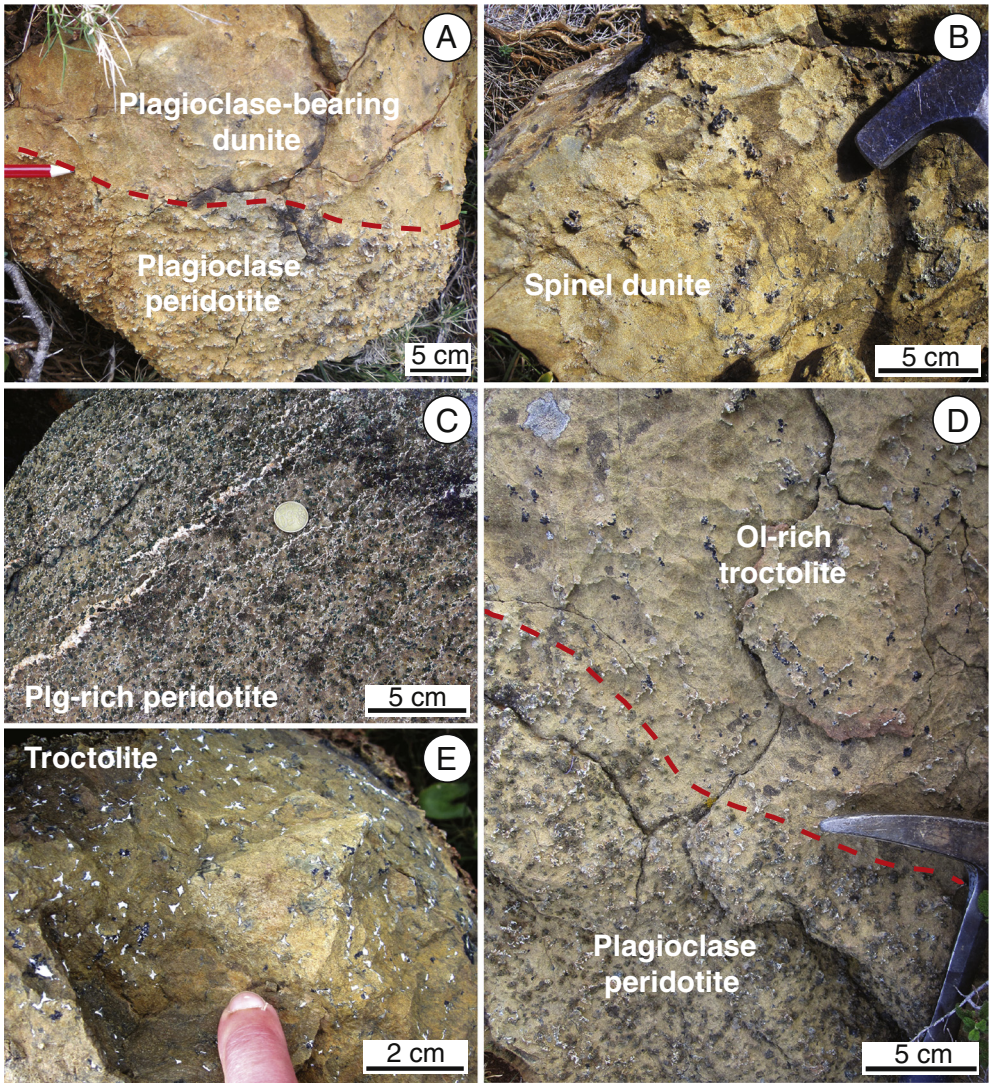

Fig. 2. Representative lithological associations of the Monte Maggiore peridotitic body. A: Plagioclase peridotite grading to plagioclase-bearing dunite; B: Spinel dunite showing spinel-rich zones; C: Strongly impregnated plagioclase peridotite, where the percolating melt segregated into gabbronoritic veinlets; D: Plagioclase peridotite grading to Ol-rich troctolite; E: Troctolite.

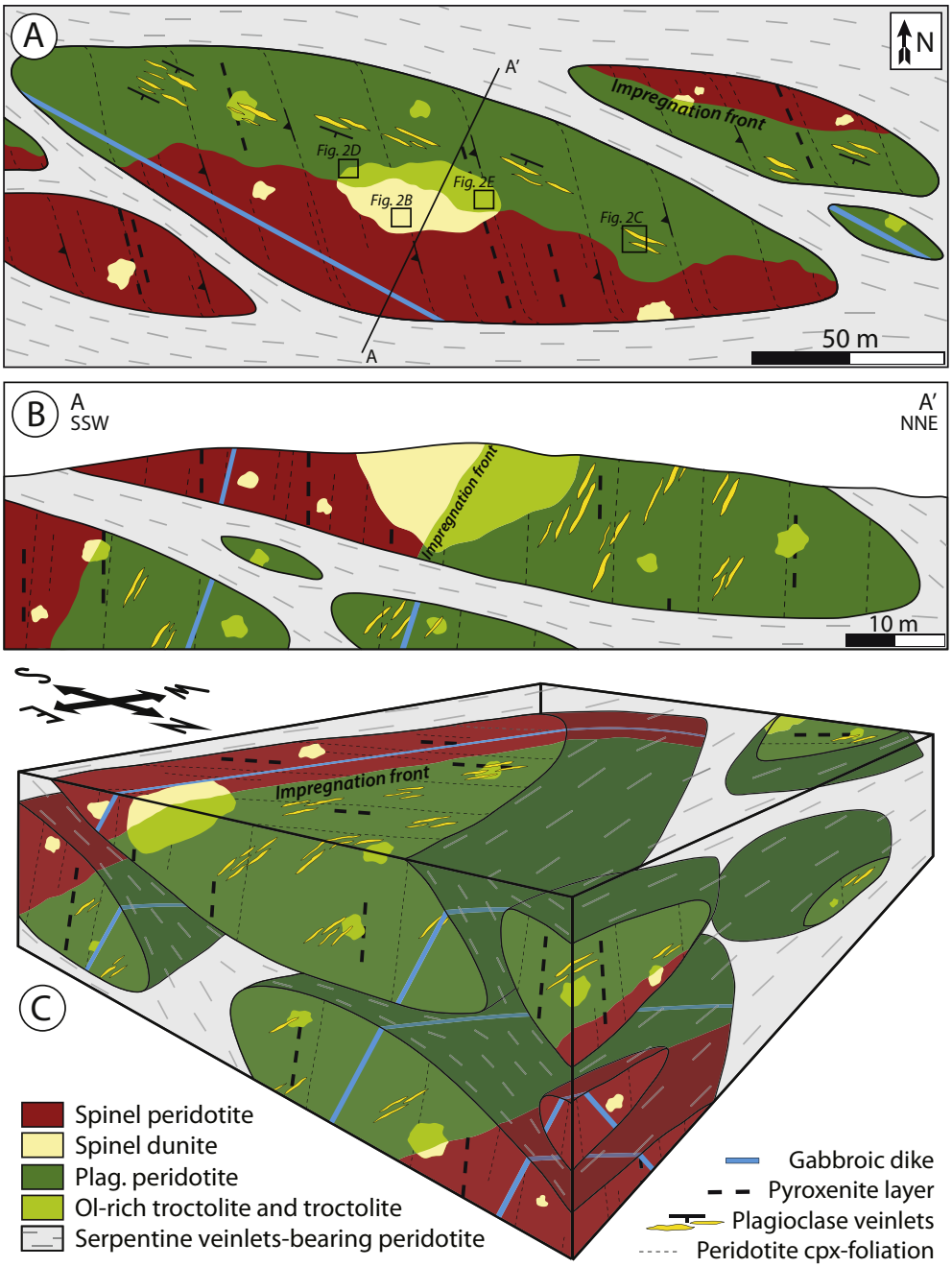

Fig. 3. A: Schematic sketch of the measured structures and lithological associations of the Mt. Maggiore peridotites in the sampling area. The black boxes locate the field observations shown in Fig. 2; B: Structural cross-section along the A-A′ line (indicated in the representative sketch); C: Three-dimensional lithological variations of the preserved spinel- and plagioclase-peridotite lenses and associated mantle structures. The impregnation front marks the contact between the spinel-facies and plagioclase-facies lithotypes.

troctolites (>75% modal olivine) and 6 troctolites (<75% modal olivine). We performed structural EBSD mapping of all samples, and mineral major (EPMA) and trace element (LA-ICP-MS) chemical analyses of 7 samples, namely 1 spinel peridotite, 1 spinel dunite, 1 plagioclase peridotite, 1 olivine-rich troctolite and 3 troctolites. Detailed methodologies for EBSD, major and trace elements analyses can be found in Supplementary Material.

5. Petrography

In granular spinel peridotites, olivine, orthopyroxene, clinopyroxene, and spinel are coarse-grained, up to centimetre-size. Olivines and pyroxenes (orthopyroxene + clinopyroxene) are deformed, and display kink bands and undulatory extinctions, respectively. Clinopyroxenes and orthopyroxenes both show thin exsolution lamellas of the complementary pyroxene. Spinel is mostly coarse-grained in the peridotite assemblage but it is also found at the rim of mantle orthopyroxene porphyroclasts, as symplectitic intergrowths of orthopyroxene + spinel ± clinopyroxene, which have been related to cooling and incorporation of the peridotites at lithospheric temperatures (970–1100 °C) (Rampone et al., 2008). Within the analyzed samples, spinel peridotites show a strong variation of modal composition of olivine, from 58% to 78% by vol. (Table 1). Melt-rock reaction microstructures, i.e. the development of undeformed olivine embayments replacing exsolved orthopyroxene and

clinopyroxene, are extensively observed in spinel peridotites with the highest modal olivine contents ("reacted spinel peridotite" in this study), as previously documented by Rampone et al. (2008) and Piccardo and Guarnieri (2010).

Spinel dunites associated to spinel peridotites are mostly characterized by a very coarse-grained texture of olivines (up to 3 cm in size), that display clear kink bands and an irregular shape. In places, coarse-grained rounded spinels (up to millimetre-size) form aligned trails within the dunite.

Spinel-bearing, plagioclase peridotites preserve locally the microstructural evidence of the first reactive melt percolation: (1) deformation and exsolution in olivine and pyroxenes, respectively; (2) olivine embayments partially replacing mantle pyroxenes and [orthopyroxene + spinel] exsolutions (Fig. 3a,b in Rampone et al., 2008). Further microstructures are indicative of melt impregnation of the spinel-bearing peridotitic matrix. Interstitial plagioclase and orthopyroxene crystallize at the expense of olivine and exsolved clinopyroxene. The most impregnated peridotites are characterized by an enrichment up to 25% of modal interstitial minerals (plagioclase + orthopyroxene ± clinopyroxene) (Table 1, Fig. 3e,f in Rampone et al., 2008). In these samples, where melt focuses to form gabbronoritic veinlets (Fig. 2c), the melt crystallizes both idiomorphic orthopyroxene and clinopyroxene at the contact between the gabbronoritic veinlet and the host peridotite, indicating that saturation of clinopyroxene is reached. These newly formed magmatic minerals are free of exsolution and deformation, and can be recognized from the mantle pyroxene relicts.

Within the replacive troctolitic bodies associated with plagioclase peridotites (Fig. 2d), the texture of the olivine matrix varies with the modal abundance of interstitial minerals. Within olivine-rich troctolites (>75% modal olivine, Figs. 4a,b, 5b), olivines are coarse-grained (up to centimetre-size), show irregular contacts and are often deformed with the occurrence of kink bands (Fig. 5). Interstitial plagioclase is found at triple grain junctions (Fig. 4a) and along olivine grain boundaries (Figs. 4b, 5c,d). Within the most impregnated troctolites (<75% modal olivine, Figs. 4c,d, 5d), some olivines show smaller grain size (millimetre-size) and are undeformed (Fig. 5d). However, troctolites still preserve coarse deformed grains of olivine (Figs. 4d and 5d) in the most dunitic areas. The plagioclase occurs as poikilitic crystals enclosing rounded small grains of olivine (Fig. 4d), and it is associated in places to poikilitic clinopyroxene.

6. Textural analysis

Microstructural observations from spinel dunite to olivine-rich troctolite to troctolite suggest a progressive variation of the texture of the olivine matrix with increasing modal composition of interstitial phases. In order to quantify the textural evolution observed in these samples, we used the EBSD maps, from which we obtain five textural parameters for each sample: (1) the number of grains, (2) the grain area (mm^2), (3) the grain aspect ratio (long axis/short axis of a grain), (4) the grain shape factor (Perimeter/Equivalent Perimeter of circle with the same area) and (5) the grain PARIS Factor (grain boundary lobateness, comparison between the perimeter of the grain and its smallest envelope; Heilbronner and Tullis, 2002; Mainprice et al., 2014; Methodology details in Supplementary Material). The aspect ratio is indicative of the crystal elongation, and the shape and PARIS factor are indicative of the tortuosity of the grain boundary. The textural parameters calculated for each sample are reported in Table 1 and are plotted in Fig. 6 against modal olivine contents. At decreasing modal olivine (from 99% vol. in the spinel dunite to 70% vol. in the troctolite) during the transition from spinel dunite to olivine-rich troctolite to troctolite, we observe a global trend of increasing number of grains (from 12 to 59), coupled to decreasing grain area (from 38 mm^2 to 6 mm^2), aspect ratio (from 1.85 to 1.43), shape factor (from 2.49 to 1.77) and PARIS factor (from 179% to 105%) (Fig. 6). This is consistent with the observed microstructural evolution from large irregular olivines in the spinel dunites to increasingly rounded small olivines in the most impregnated troctolites (Figs. 4 and 5). Similar textural

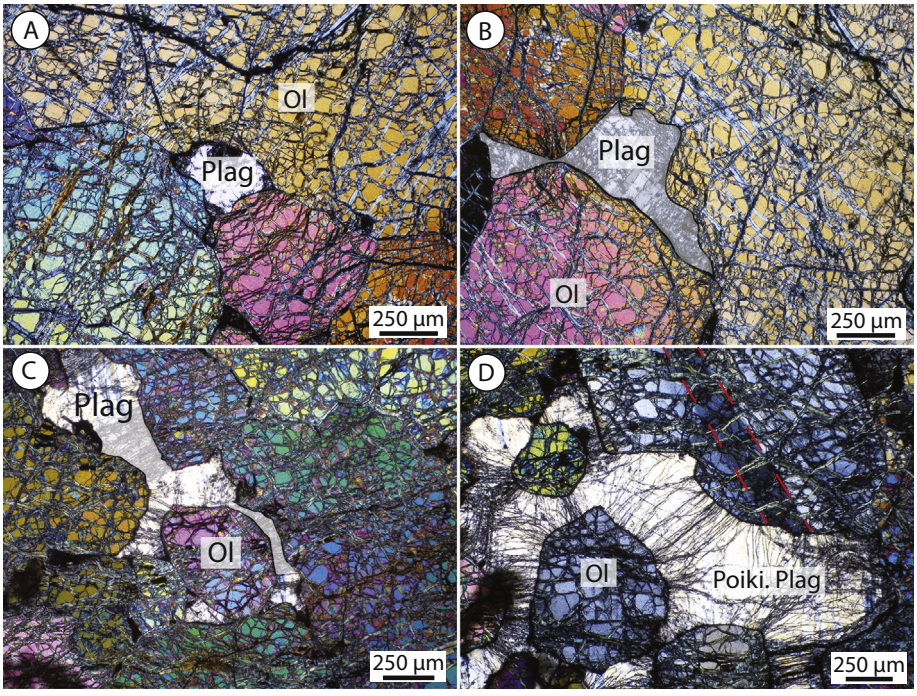

Fig. 4. Microstructural evolution with increasing impregnation of a spinel dunite. A: Ol-rich troctolite, plagioclase crystallized at the triple grain junction, and partly corroded pre-existing olivine; B: Ol-rich troctolite, plagioclase corroded olivine along grain boundaries; C: Troctolite, interstitial to poikilitic plagioclase surrounds smaller olivine grains; D: Troctolite, poikilitic plagioclase includes rounded olivines. In the top left corner, an olivine is almost completely disrupted into two different rounded grains. The dashed red lines highlight a kink band in a coarse deformed olivine.

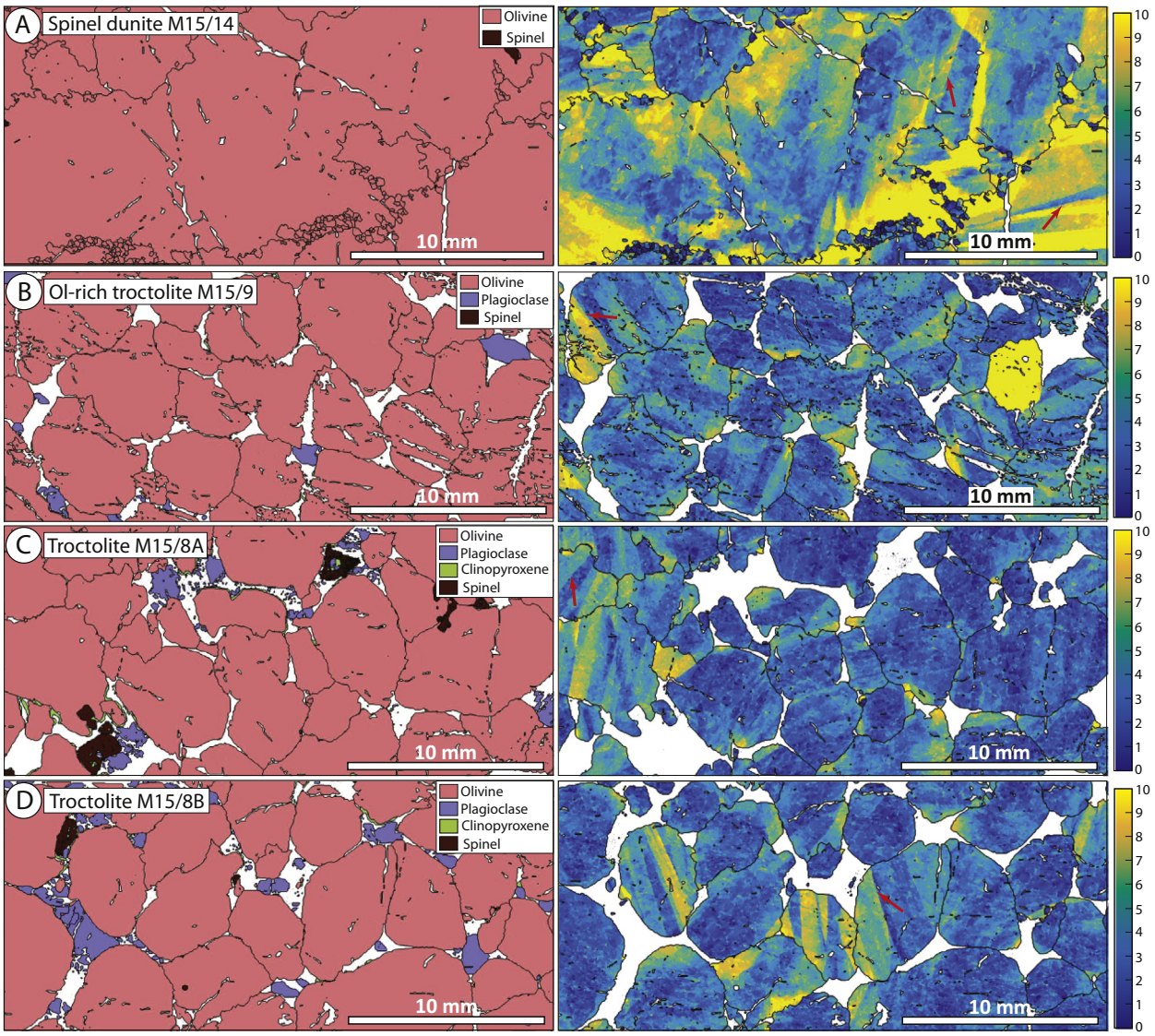

Fig. 5. EBSD phase (left column) and misorientation (right column) maps showing the textural evolution of the olivine matrix with ongoing impregnation (decreasing modal olivine from A to D). A: Spinel dunite M15–14, 99% olivine; B: Ol-rich troctolite M15–9, 85% olivine; C: Troctolite M15-8A, 73% olivine; D: Troctolite M15-8B, 73% olivine. White areas in the phase maps are non-indexed pixels (mostly due to alteration of olivine and plagioclase). The 0–10° scale indicates misorientation from the average orientation of a grain, and the red arrows point to kink bands within deformed olivines.

evolution was described by Boudier (1991) in the Oman ophiolite mantle-crust transition zone, to explain the replacive formation of wehrlites at the expense of dunites. The high values of PARIS factor (>100%; Table 1) are likely a consequence of the serpentinization of the olivine, leading to an indentation of the grain boundary and therefore to an over-estimation of the analyzed grain perimeter and calculated PARIS factor. However, the small-scale serpentinization does not impact the global decreasing trend at decreasing modal olivine content, and the PARIS factor shows an evolution consistent with the shape factor during the transition from spinel dunite to olivine-rich troctolite to troctolite.

7. Crystallographic Preferred Orientation of olivine

The Mt. Maggiore peridotites, dunites, olivine-rich troctolites and troctolites all show clear Crystallographic Preferred Orientation patterns. However, they are characterized by a very coarse centimetric grain size, therefore the low number of grains does not enable the quantification of the CPO strength by the J-index, defined as the volume-averaged integral of the squared orientation densities, sensitive to peaks in the orientation distribution function (i.e. single grains when only a few olivine crystals are analyzed; Bunge, 1982; Ben Ismail and Mainprice, 1998). Olivine CPO are thus used as qualitative indicators of first-order structural variations between the analyzed lithologies. The interstitial minerals are mainly poikilitic and a single crystal can cover almost the entire thin section, it is thus impossible to measure any CPO for plagioclase, orthopyroxene and clinopyroxene crystallized from the impregnating melt. Representative olivine CPO, BA-index (representative of the CPO symmetry of the olivine [100] and [010] axes; Mainprice et al., 2014), Grain Orientation Spread (GOS) and 2–10° misorientation rotation axes for each described lithotype (spinel peridotite, reacted spinel peridotite, spinel dunite, plagioclase peridotite, olivine-rich troctolite, troctolite) are shown in Fig. 7, and the full olivine CPO dataset is given in Supplementary Fig. S1.

Olivine in both unreacted spinel peridotite (Fig. 7a) and plagioclase peridotite (Fig. 7d) are characterized by an axial-[100] CPO (BA-index > 0.7; Mainprice et al., 2014; Tommasi and Ishikawa, 2014), with [100] axis showing the strongest preferred orientation in the foliation plane, [010]

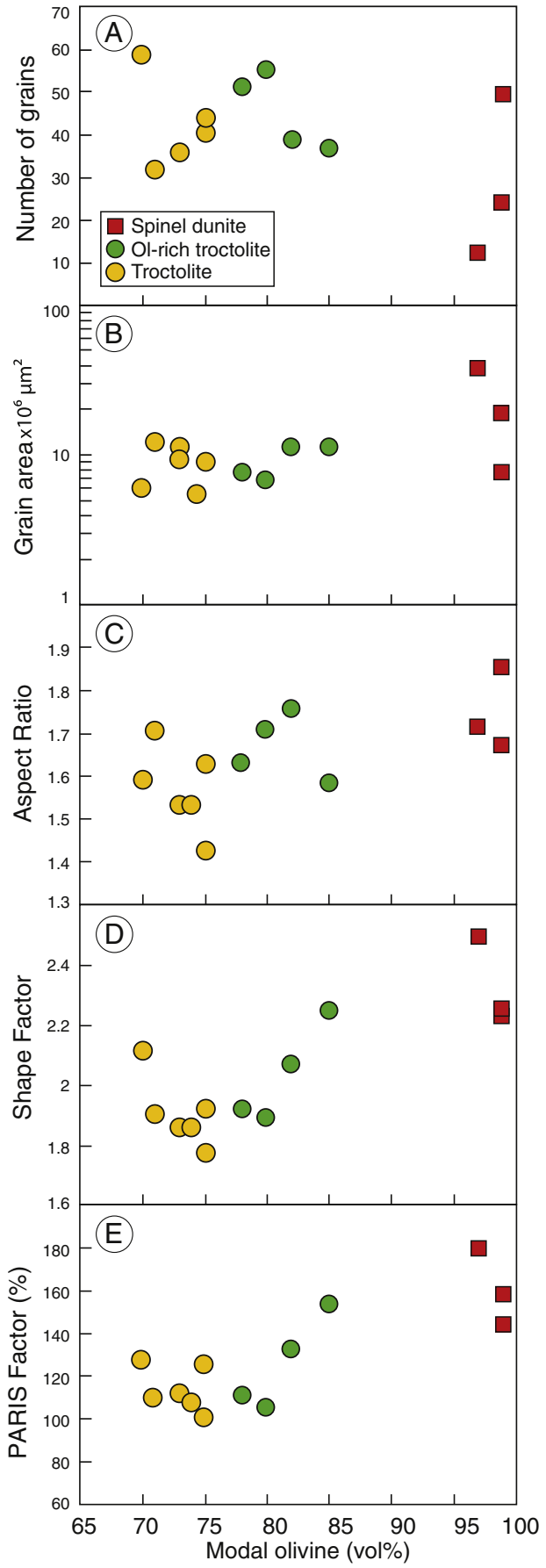

axis maximum oriented normal to the foliation plane, and [001] maximum within the foliation plane. The dominant low-angle misorientations within olivines are accommodated by both [001] and [010] rotation axes, with a maximum on [001] (Fig. 7). This indicates that plastic deformation of olivine crystals was related to dislocation creep with activation of (010)[100] slip system, the easiest at high temperatures conditions (1100–1200 °C), and (001)[100], another commonly observed slip system activated at high temperature in olivine (Ben Ismail and Mainprice, 1998; Drouin et al., 2010; Higgie and Tommasi, 2012; Karato et al., 2008; Tommasi et al., 2000). When available in spinel peridotites, orthopyroxene CPO shows strongest concentrations of the [001] axis, sub-parallel to the olivine [100] crystallographic axis and to the foliation. It is indicative of the activation of (100)[001] orthopyroxene slip system, consistently with high temperature dislocation creep (Karato et al., 2008; Soustelle et al., 2009; Tommasi et al., 2000).

Olivines in the reacted spinel peridotite (Fig. 7b), spinel dunite (Fig. 7c), olivine-rich troctolite (Fig. 7e) and troctolite (Fig. 7f) are characterized by an axial-[010] CPO (BA-index < 0.45; Mainprice et al., 2014; Tommasi and Ishikawa, 2014), with the strongest axis orientation being [010] normal to the foliation. Axial-[010] CPO have been previously described in impregnated peridotites (Ben Ismail et al., 2001; Le Roux et al., 2008; Tommasi et al., 2008), hybrid olivine-rich gabbroic rocks (Higgie and Tommasi, 2012, 2014), and experiments of melt segregation during deformation (Holtzman et al., 2003). The development of such patterns has been explained by: (1) activation of dominant (010)[100], together with (010)[001] slip systems (Mainprice et al., 2005; Tommasi et al., 2000); (2) 3D deformation involving stretching in multiple directions in the foliation plane (Tommasi et al., 1999); (3) static recrystallization (Tommasi et al., 2008); and (4) deformation in presence of melt (Holtzman et al., 2003; Kaczmarek and Tommasi, 2011; Le Roux et al., 2008) (see Discussion below). The low-angle misorientations (2–10°) of olivine in these lithotypes are mainly accommodated by [010] rotation axis (Fig. 7). From spinel dunite to olivine-rich troctolite and troctolite, we observe a randomization of the orientation of the [100] axis, and a decrease in the Grain Orientation Spread (average misorientation to the mean orientation) of olivine (from 3.61 to 2.71) and in the concentration of the misorientation along [010] olivine axis (Fig. 7).

8. Major and trace elements mineral compositions

Major and trace elements compositions of minerals in the studied spinel peridotite, plagioclase peridotite, spinel dunite, olivine-rich troctolite, and troctolites are reported in Tables S2–S6 of Supplementary Material. The standard deviations of the mineral trace elements analyses are reported in Table S7 of Supplementary Material. Overall, our data are consistent with mineral compositions reported in previous studies on the Mt. Maggiore peridotitic body (Müntener and Piccardo, 2003; Piccardo and Guarnieri, 2010; Rampone et al., 1997, 2008), except for the trace element abundances of olivine, which constitute an entirely new data set.

Olivines from spinel peridotites, plagioclase peridotites, spinel dunites, olivine-rich troctolites and troctolites show homogeneous major elements compositions at high Forsterite (Fo = 89.4–90.2) and Ni (2514–3064 ppm) contents (Table S2). However, variations in trace elements concentrations are observed between the described lithotypes. Olivines in spinel peridotites show low contents of Ti (10–15 ppm), Y (0.01–0.02 ppm) and Zr (0.002–0.003 ppm), whereas higher contents in these elements (e.g. Ti = 41–94 ppm) at constant Fo values are observed in olivines from dunite, olivine-rich troctolite and troctolite (Fig. 8). Olivine REE patterns show a significant variability between

Fig. 6. Evolution of textural parameters of olivine plotted against the modal composition of olivine in samples from spinel dunite to Ol-rich troctolite and troctolite. A: Number of grains; B: Grain area; C: Aspect Ratio; D: Shape Factor; E: PARIS Factor.

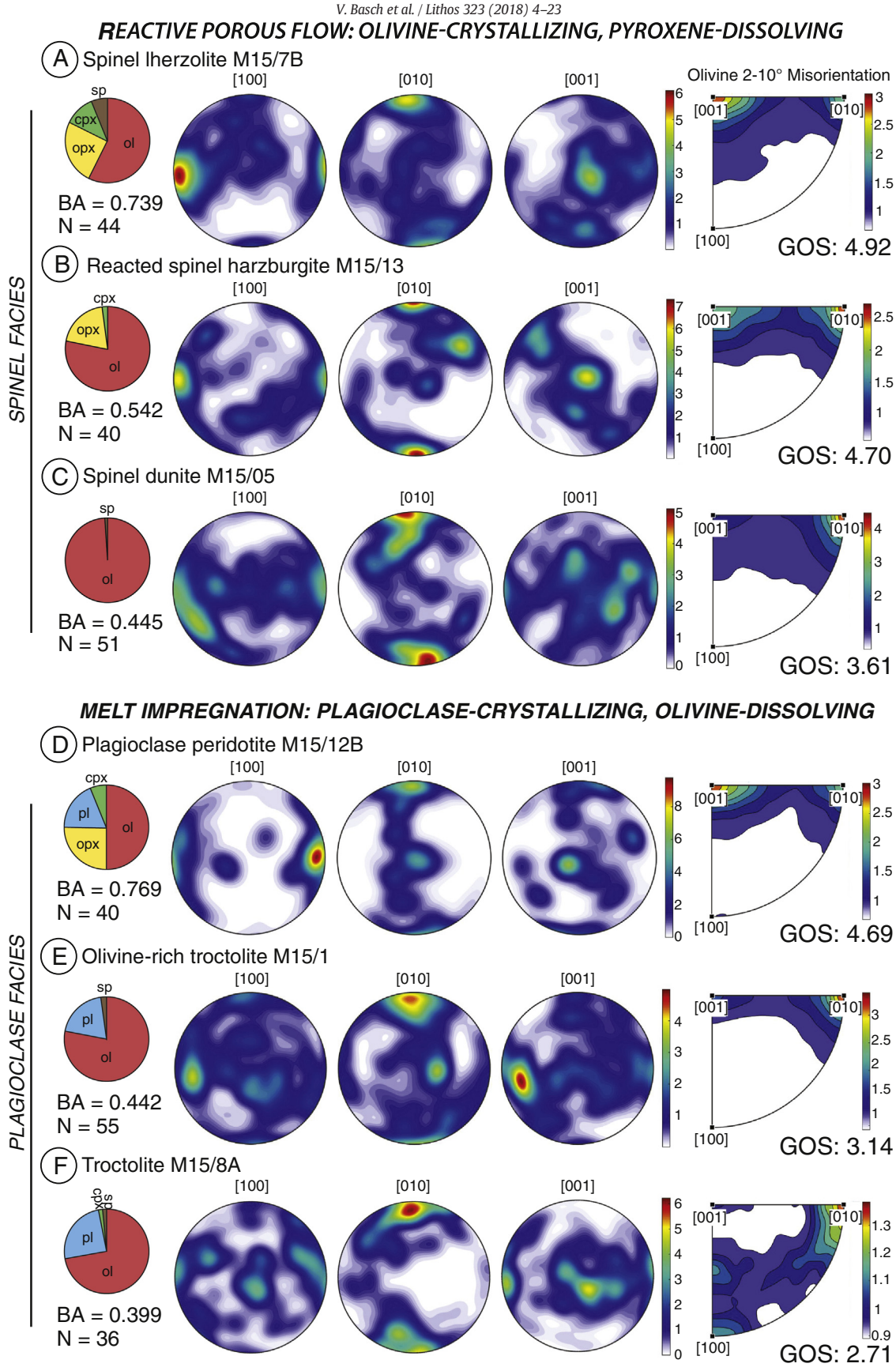

Fig. 7. Representative olivine Crystallographic Preferred Orientation and 2–10° misorientation Inverse Pole Figures of the described lithotypes from Mt. Maggiore peridotitic body. One-point-per-grain equal-area, lower hemisphere stereographic projections. The colour bar is scaled to the maximum concentration of the three crystallographic axes. A: Spinel lherzolite M15/7B; B: Reacted spinel harzburgite M15/13; C: Spinel dunite M15/05; D: Plagioclase peridotite M15/12B; E: Olivine-rich troctolite M15/1; F: Troctolite M15/8A. BA refers to the calculated BA-index, N is the number of olivine grains, and GOS refers to the Grain Orientation Spread.

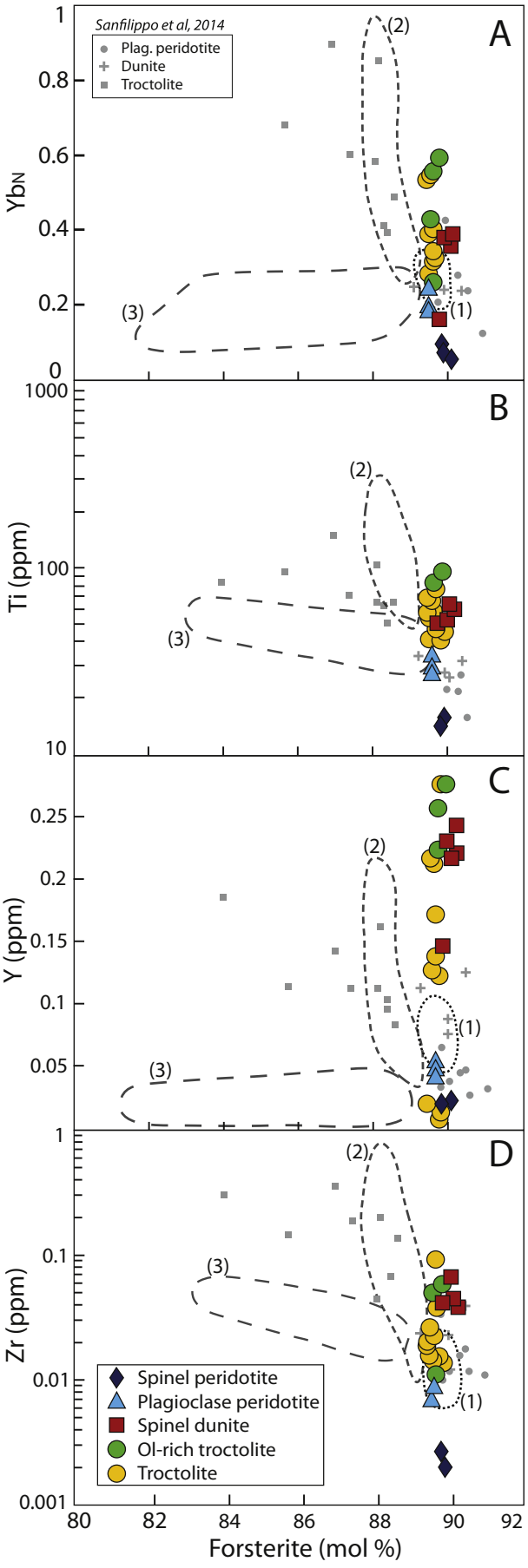

Fig. 8. Forsterite (mol%) vs selected trace elements in olivine. A: Yb normalized to C1-chondrite, normalizing values after Sun and McDonough (1989); B: Ti (ppm); C: Y (ppm); D: Zr (ppm). Compositional fields after Rampone et al. (2016); (1) Peridotites, (2) Troctolites, (3) Olivine gabbros; and single analyses from Sanfilippo et al. (2014).

the analyzed lithotypes (Figs. 9a,b, 10a,b). Olivines in spinel peridotites show low HREE abundances (Yb_N = 0.05–0.095 times C1), and high HREE fractionation (Dy_N/Yb_N = 0.05–0.08), comparable to olivines from the Gakkel Ridge lherzolites reported by D'Errico et al. (2016). Olivines in the plagioclase peridotite show higher REE absolute concentrations (Yb_N = 0.18–0.25 times C1) at constant HREE fractionation (Dy_N/Yb_N = 0.05–0.07). In the spinel dunite, olivines show higher REE abundances relative to olivines in peridotites (Yb_N = 0.3–0.38 times C1). In terms of HREE, they resemble olivines in olivine-rich troctolites from Mid-Atlantic Ridge (Drouin et al., 2009) and Erro-Tobbio (Rampone et al., 2016), but they display lower MREE/HREE fractionation (Dy_N/Yb_N = 0.26–0.43). Olivines from olivine-rich troctolite and troctolites have similar REE composition. They also show enriched HREE absolute concentrations (Yb_N = 0.26–0.59), but at stronger HREE fractionation (Dy_N/Yb_N = 0.10–0.19).

Clinopyroxenes in the spinel peridotite, plagioclase peridotite and troctolite show similar Mg-value interval (Mg# = 88.7–91.4) to clinopyroxenes analyzed in the same lithotypes by Rampone et al. (1997, 2008) (Table S3). Variations are observed in Ti and Al concentrations between lithotypes, with low Ti (TiO_2 = 0.20–0.29 wt%) and high Al (Al_2O_3 = 5.71–6.46 wt%) concentrations in spinel peridotites, and higher Ti (TiO_2 = 0.23–0.62 wt%) and lower Al (Al_2O_3 = 3.39–6.02 wt%) concentrations in plagioclase peridotite. As documented by Rampone et al. (1997, 2008), clinopyroxene porphyroclasts in the plagioclase peridotites show a high compositional variability from core to rim. Cores preserve the low-Ti, high-Al signature, similar to the composition of clinopyroxenes porphyroclasts in spinel peridotites, whereas the rims show higher Ti, and lower Al contents. A similar zoning is observed in interstitial and poikilitic clinopyroxene from the troctolite, from relatively low-Ti (TiO_2 = 0.29–0.41 wt%), and high-Al (Al_2O_3 = 5.2–5.7 wt%) cores to high-Ti (TiO_2 = 0.44–0.91 wt%), and low-Al (Al_2O_3 = 3.83–4.94 wt%) rims. In both spinel and plagioclase peridotites, clinopyroxenes show strong LREE depletion (Ce_N/Yb_N = 0.018–0.044), and flat MREE-HREE patterns (Figs. 9c, 10c) comparable to clinopyroxene compositions reported in depleted lherzolites from the Gakkel Ridge (D'Errico et al., 2016). Higher HREE absolute compositions have been measured in clinopyroxene cores from plagioclase peridotites (Yb_N = 7–12 times C1). Clinopyroxenes in troctolites also exhibit significant LREE depletion (Ce_N/Yb_N = 0.015–0.043). In all plagioclase-bearing lithotypes (peridotite and troctolite) the rims of clinopyroxene show an enrichment in Ti, Sc, V, Y and MREE-HREE (Yb_N = 12–15 times C1), the development of convex-upward REE patterns and Eu negative anomalies, as previously documented by Rampone et al. (2008) and Piccardo and Guarnieri (2010).

Plagioclase in the plagioclase peridotite, olivine-rich troctolite and troctolite show high Anorthite contents (An = 85.1–88.1) and very low Sr abundances (15.5–24.6 ppm), as previously documented by Rampone et al. (1997, 2008) and Piccardo and Guarnieri (2010) (Table S4). In all studied samples, REE patterns of plagioclase are characterized by significant and similar LREE depletion (Ce_N/Sm_N = 0.19–0.49). However, variations in absolute REE concentrations are observed between the different lithotypes. The lowest abundances are observed in plagioclase of plagioclase peridotites (e.g. Sm_N = 0.2–0.4 times C1), whereas they progressively increase in troctolites (Sm_N = 0.4–1.2 times C1) and olivine-rich troctolites (Sm_N = 0.7–1.5 times C1).

Orthopyroxene is only found in the spinel and plagioclase peridotites. It shows homogeneous Mg-values (Mg# = 89.2–90.3) in both lithotypes (Table S5). As observed for clinopyroxene, the REE absolute concentrations of orthopyroxenes in the spinel peridotite (Yb_N = 1.9–2.5 times C1, Ce_N/Yb_N = 0.002–0.006) are comparable to those of

orthopyroxenes in the Gakkel Ridge depleted lherzolites (D'Errico et al., 2016) (Figs. 9f, 10f). In the plagioclase peridotite, orthopyroxenes show higher absolute REE concentrations (Yb_N = 2.3–5 times C1) at similar REE fractionation (Ce_N/Yb_N = 0.002–0.004). They are consistent with orthopyroxene compositions documented by the previous study of Rampone et al. (2008).

Spinel in the troctolite show lower Mg-values (Mg# = 60.2–66.7) and higher Cr-values (Cr# = 34.7–44.9) and TiO_2 (TiO_2 = 0.53–0.85 wt%) than spinel analyzed in the spinel peridotite (Mg# = 73.8; Cr# = 24.2; TiO_2 = 0.11 wt%) (Table S6). In the spinel dunite, spinels show intermediate compositions (Mg# = 64.3–69.4; Cr# = 27.3–36.4; TiO_2 = 0.40–0.84 wt%) between the spinel peridotite and the troctolite. Spinels analyzed in the troctolite show higher Mg-values and lower Cr-values and TiO_2 contents than spinels analyzed in olivine-rich troctolites in oceanic (Drouin et al., 2009; Suhr et al., 2008) and ophiolitic settings (Renna et al., 2016; Renna and Tribuzio, 2011).

9. Discussion

9.1. Origin of replacive dunites by spinel-facies reactive porous flow

As reported in previous studies, the Mt. Maggiore peridotitic body records an olivine-crystallizing, pyroxene-dissolving reactive melt percolation stage at spinel facies conditions (Müntener and Piccardo, 2003; Piccardo and Guarnieri, 2010; Rampone et al., 1997, 2008). This melt-rock interaction is documented by the development of olivine embayments replacing mantle pyroxenes, and the partial dissolution of pyroxenite layers commonly associated with the peridotites. The reacted lithotypes show a high modal variability, from depleted spinel lherzolites to pyroxene-poor harzburgites until the formation of dunite bodies in the most extensively reacted peridotites. The dunitic bodies are characterized by irregular to straight contacts with the spinel peridotite (Fig. 2a) and show in places spinel trails that suggest the former

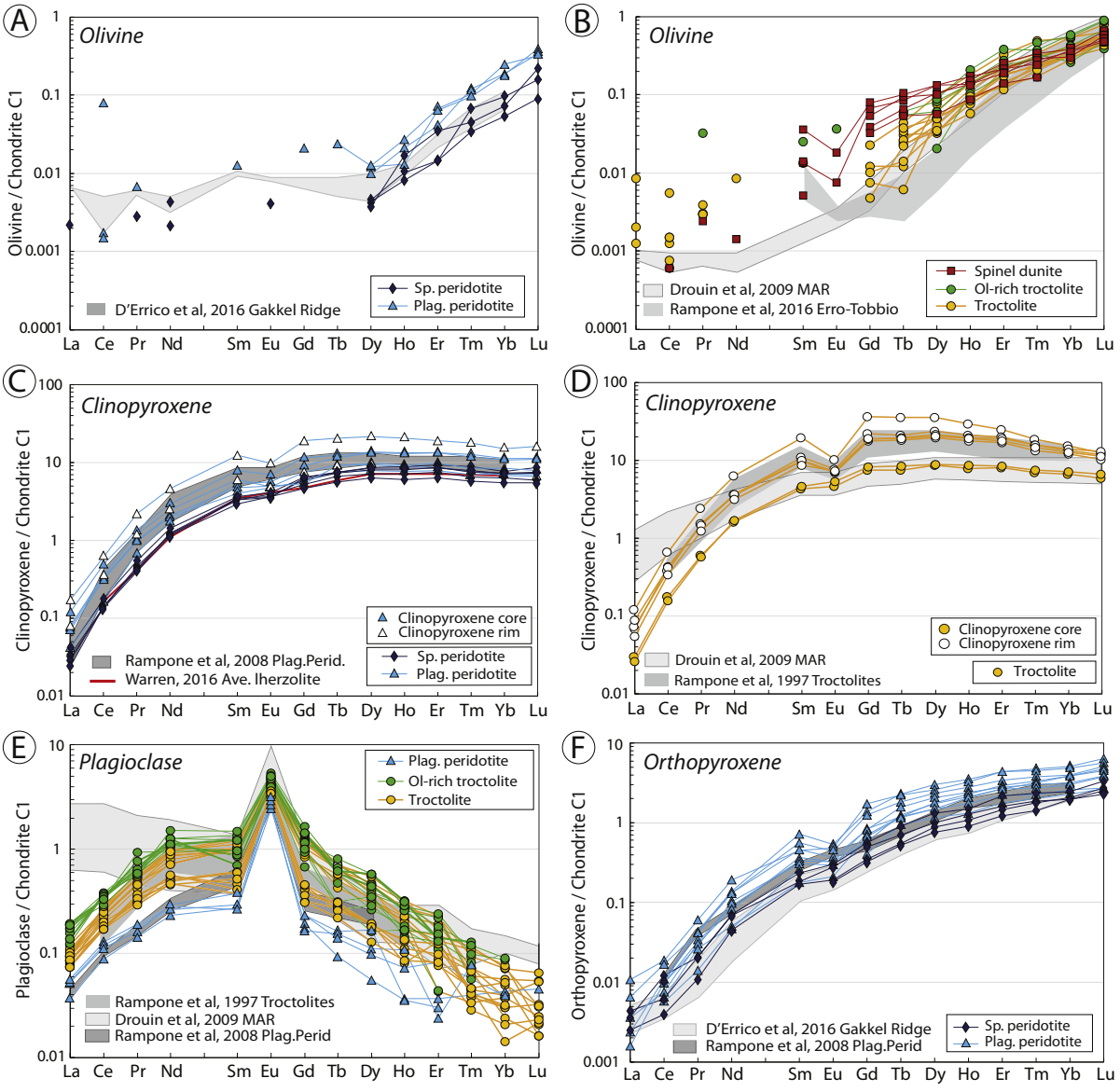

Fig. 9. C1-normalized REE composition of rock-forming minerals. A: Olivine in spinel and plagioclase peridotite; B: Olivine in spinel dunite, Ol-rich troctolite and troctolite; C: Clinopyroxene in spinel and plagioclase peridotite; D: Clinopyroxene in troctolite; E: Plagioclase; F: Orthopyroxene. C1-chondrite normalization values after Sun and McDonough (1989). The compositional fields represent Gakkel Ridge abyssal lherzolites from D'Errico et al. (2016), Mid-Atlantic Ridge olivine-rich troctolites from Drouin et al. (2009), Erro Tobbio ophiolitic troctolites from Rampone et al. (2016), and Mt. Maggiore plagioclase peridotites and troctolites from Rampone et al. (1997, 2008). The solid red line is the average of the residual lherzolite field after Warren (2016). For clinopyroxene, a distinction is made between cores (full symbol) and rims (empty symbols) of crystals.

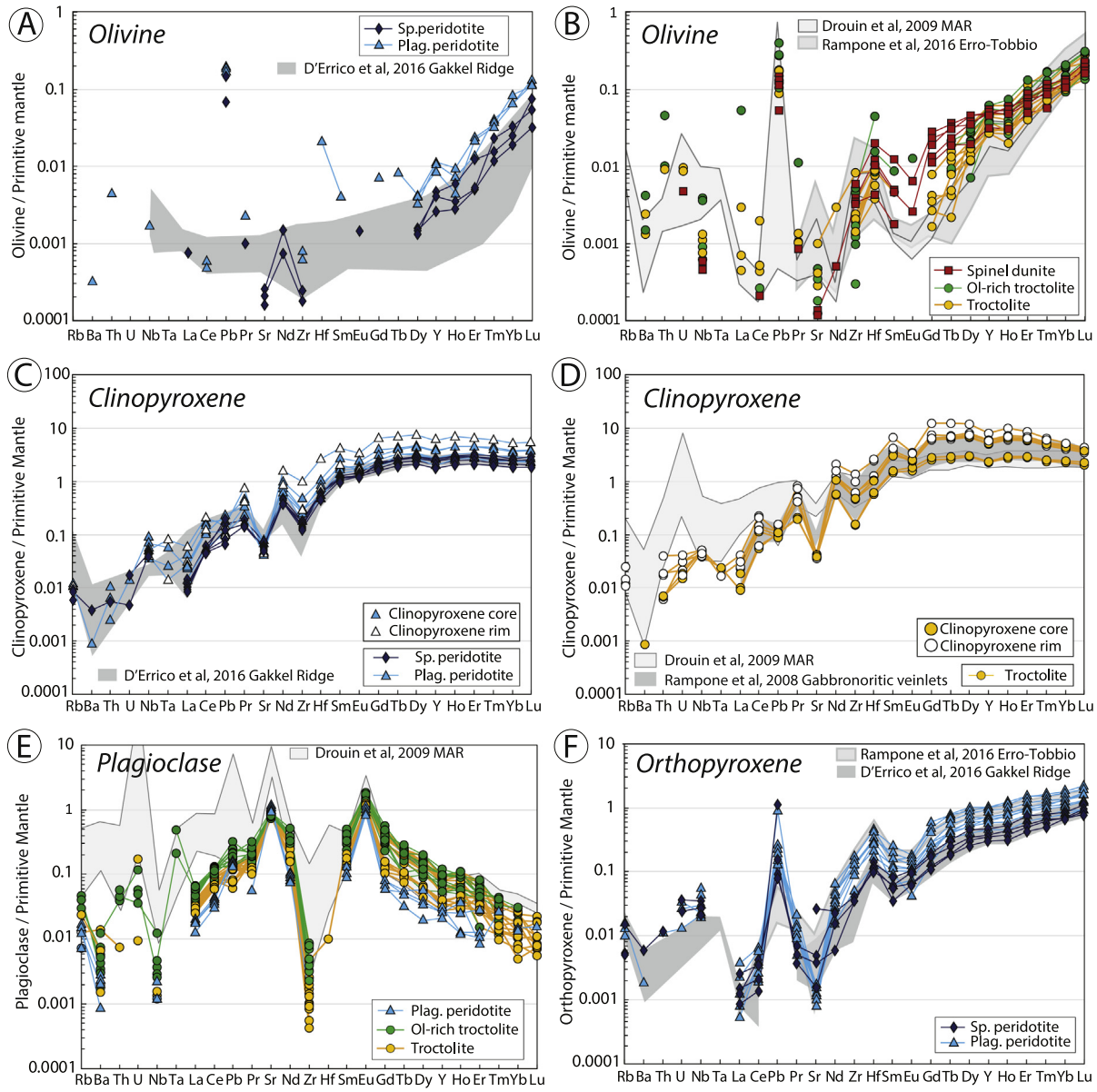

Fig. 10. Primitive Mantle-normalized trace elements compositions of the rock-forming minerals. A: Olivine in spinel and plagioclase peridotite; B: Olivine in spinel dunite, Ol-rich troctolite and troctolite; C: Clinopyroxene in spinel and plagioclase peridotite; D: Clinopyroxene in troctolite; E: Plagioclase; F: Orthopyroxene. Primitive Mantle normalization values are after Sun and McDonough (1989). The compositional fields are similar to Fig. 9. For Clinopyroxene, a distinction is made between cores (full symbol) and rims (empty symbols) of crystals.

presence of a pyroxenite layer, completely dissolved during extensive reactive porous flow (Piccardo and Guarnieri, 2010) (Fig. 2b). Despite the high modal variability during evolution from spinel lherzolite to reacted harzburgite to spinel dunite, Rampone et al. (2008) reported rather constant bulk-rock Mg-values (Mg# = 89.8–90.5), and olivines accordingly define a very narrow range of $Fo_{89.4–90.2}$ content variation. Constant bulk Mg-values at increasing modal olivine follow reactive porous flow trends (Rampone et al., 2008) and are indicative of a buffering of the percolating melt at Mg# ≈ 75 (i.e. in equilibrium with olivine Fo_{90}, Collier and Kelemen, 2010) during reactive porous flow. All lines of evidence point to a replacive origin of the dunites in the Mt. Maggiore peridotitic body. In the following, we discuss the structural and geochemical variability of the olivine matrix accompanying the observed evolution from spinel lherzolites to spinel harzburgites to spinel dunites.

9.1.1. Structural evolution during dunitization

The replacive formation of the dunitic bodies is driven by an olivine-crystallizing, pyroxene-dissolving reactive porous flow in the spinel lherzolites. The modal olivine enrichment from spinel lherzolites to reacted spinel peridotites to spinel dunites is observed with the growth of the pre-existing olivines at the expense of ortho- and clinopyroxene, through the development of olivine embayments corroding mantle pyroxenes. The growth of olivine is confirmed by the observed olivine texture in the spinel dunites, namely very coarse grains of olivine (up to 3 cm in size, Fig. 6b), showing irregular shapes (Fig. 6d).

During the evolution from spinel lherzolite to reacted spinel peridotite to spinel dunite (Fig. 7a,b,c), the olivine CPO progressively varies from an axial-[100] CPO in the spinel lherzolite to an axial-[010] CPO in the spinel dunite, consistently with the decreasing BA-index from BA = 0.74 in the spinel peridotites to BA = 0.45 in the spine dunite. Axial-[100] olivine CPO is largely described in natural peridotites (Soustelle et al., 2009, 2010; Tommasi et al., 2000) as the result of dislocation creep and the joint activation of (010)[100] and (001)[100], the two easiest slip systems in olivine at asthenospheric conditions (Tommasi et al., 2000).

The analyzed axial-[010] CPO in the spinel dunite is consistent with previously reported olivine CPO in replacive dunites from French Polynesia xenoliths (Tommasi et al., 2004). An axial-[010] CPO of olivine can be formed by the joint activation of dominant (010)[100], together with (010)[001] slip system (Mainprice et al., 2005; Tommasi et al., 2000), dominantly activated at low temperatures (<900 °C; Carter and Avé Lallemant, 1970), high pressures and/or water contents (>3 GPa; Jung and Karato, 2001; Jung et al., 2009). However, no hydrous minerals (such as amphibole) have been observed within our samples, and the Mt. Maggiore peridotites display microstructural evidence that the reactive melt percolation forming replacive dunites occurred at lithospheric temperatures and spinel facies depths (T = 970–1100 °C; Rampone et al., 2008; Piccardo and Guarnieri, 2010). Therefore, it is unlikely that the pressure-temperature conditions and/or water contents, leading to activation of [001] glide in olivine (Jung et al., 2009; Jung and Karato, 2001; Mainprice et al., 2005), are the dominant parameters accounting for the observed olivine CPO in the spinel dunites. Olivines in the Mt. Maggiore dunites are deformed, irregular and very coarse-grained, thus the development of axial-[010] CPO is not likely to be related to static recrystallization, as proposed by Tommasi et al. (2008). Field and microstructural evidence support the formation of dunites after extensive pyroxene-dissolving, olivine-crystallizing melt-rock interaction. Accordingly, we infer that the CPO evolution observed in olivine from spinel lherzolite (axial-[100]) to spinel dunite (axial-[010]) is due to deformation in presence of melt, as was described in melt-bearing experiments of deformation (Holtzman et al., 2003) and in the Lherz refertilized peridotites (Le Roux et al., 2008). Dunitic zones correspond to the most reacted lithotype, thus to the strongest accumulation of melts over time. However, the preservation of a clear olivine CPO implies that the instantaneous melt/rock ratio remained, during the whole process of reactive porous flow, below the critical value allowing for loss of cohesion of the solid matrix (20–40%; Rosenberg and Handy, 2005). The reacted spinel harzburgite (Fig. 7b) is characterized by a transitional CPO of olivine, between the spinel lherzolite (Fig. 7a) and the spinel dunite (Fig. 7c), with a decreasing concentration of the [100] axis and increasing concentration of [010]. This is indicative of a progressive change of the CPO, as a function of the cumulated melt fraction and strain (Higgie and Tommasi, 2012).

A change in the rotation axes accommodating the low-angle misorientations (<10°) within olivine crystals is observed during the dunitization process. Olivines in spinel lherzolites and spinel dunites show low-angle misorientation accommodated by both [001] and [010] rotation axes, with major accommodation by [001] axis for olivines in spinel lherzolites and major accommodation by [010] axis for olivines in spinel dunites. This variation can be ascribed to a change in the preferential slip system activation of olivine, from (010)[100] to (001)[100] in spinel peridotites and spinel dunites, respectively (Tommasi et al., 2000).

9.1.2. Chemical changes of percolating melt: REE modelling

No significant major and minor elements compositional variability is observed in olivines from spinel peridotites and spinel dunites (Fo = 89.4–90.2, Ni = 2500–3000 ppm). On the other hand, olivines in the spinel dunites are characterized by much higher incompatible trace elements contents (e.g. Ti, Zr, Y, Fig. 8) with respect to olivines in the spinel peridotites. Also, they show higher absolute REE concentrations (Yb_N = 0.3–0.38 times C1) coupled to lower MREE/HREE fractionation (Dy_N/Yb_N = 0.26–0.43) than olivines in spinel peridotites (Yb_N = 0.05–0.095 times C1; Dy_N/Yb_N = 0.05–0.08) (Figs. 9a,b, 10a,b). In terms of such trace elements, olivines in the spinel dunites more closely resemble olivines in the troctolites, although bearing a different MREE/HREE fractionation (Fig. 9b).

To better understand the trace element variability related to the described process of reactive melt percolation at spinel facies, we performed a geochemical modelling using Plate Model numerical simulations (Vernières et al., 1997). This model reproduces a rock-dominated reactive melt percolation, during which the composition of the melt is buffered by the solid matrix, varying porosity and modal composition along the percolation column (Fig. 11). The selected host rock forming the mantle column is the depleted spinel lherzolite MM2/12 from Rampone et al. (2008), whose modal composition (Ol:Opx:Cpx = 0.74:0.20:0.06) is similar to spinel peridotites analyzed in this study (Table 1). The spinel peridotites from Mt. Maggiore were previously interpreted as residual

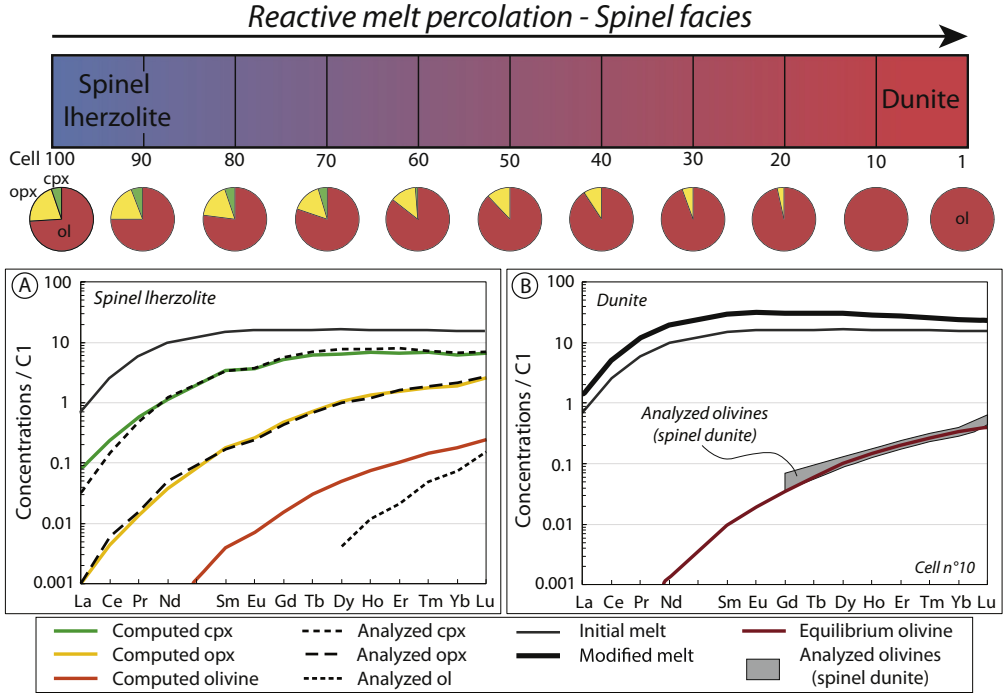

Fig. 11. Evolution of chondrite-normalized REE abundances and modal compositions computed by numerical simulation (Plate model, Vernières et al., 1997) during a process of reactive melt percolation at spinel facies. Detail of input parameters is given in the text. C1-chondrite normalization values are after Sun and McDonough (1989). A: initial stage, spinel lherzolite; B: dunite formed after reactive melt percolation.

peridotites (Piccardo and Guarnieri, 2010; Rampone et al., 1997, 2008) after 6% fractional melting, following the equation of Johnson et al. (1990) and Warren (2016). Rampone et al. (1997, 2008), using simple AFC modelling, inferred that melts percolating the spinel and plagioclase peridotites (after the partial melting event) had also a LREE-depleted chemical signature. They hypothesized that such depleted signature could either represent a primary characteristic of the melt, or it was acquired during the reactive melt percolation through the depleted spinel lherzolite (Rampone et al., 2008).

We performed the Plate Model numerical simulations (Vernières et al., 1997) with different, variably LREE-depleted, initial melts. We noticed that an N-MORB starting composition (Workman and Hart, 2005) although reproducing the MREE/HREE fractionation and absolute concentrations of olivine in the spinel dunite, does not explain the strong LREE-depletion of plagioclase and clinopyroxene analyzed in the plagioclase peridotite and troctolite (Fig. S2). This observation, together with the evidence of preserved LREE-depleted compositions of reacted spinel peridotites (Rampone et al., 2008), corroborate the inference that the percolating melts had likely a primary LREE-depleted signature. Accordingly, we selected an initial melt composition corresponding to a depleted single melt increment obtained after 6% fractional melting of a slightly depleted mantle source, consistent with previous assumptions (Piccardo and Guarnieri, 2010; Rampone et al., 1997, 2008) (Fig. 11a, Table S8). In order to model the reactive percolation leading to the replacive formation of the dunites, we assumed the following reaction:

$$0.6\ opx_1 + 0.4\ cpx_1 + melt_1 = olivine_2 + melt_2$$

in which mantle pyroxenes (M_a = 60% opx + 40% cpx) are dissolved by the incoming melt ($melt_1$), while crystallizing olivine (M_c = 100% olivine), at global $[M_a/M_c] = 1.08$. The partition coefficients used for olivine, orthopyroxene and clinopyroxene, after Warren (2016), are reported in Table S8. The computed initial REE trace element compositions of clinopyroxene and orthopyroxene in the host depleted lherzolite fit well the analyzed mineral compositions (Fig. 11a), whereas discrepancies are observed between computed and analyzed olivine REE compositions, both in terms of absolute concentrations and fractionation (Fig. 11a). We infer that the lower trace element abundances and stronger fractionation observed in the analyzed olivine in spinel peridotite is the result of subsolidus reequilibration between clinopyroxene and olivine, as described by Sun and Liang (2014). Calculated olivine–clinopyroxene REE partitioning (Sun and Liang, 2012, 2013a, b, 2014) yield low equilibrium temperature of 1000–1100 °C (Fig. S3), consistent with the low equilibration temperature (970–1100 °C) calculated by different geothermometers (Ca in opx, Sc and V opx-cpx partitioning; see Rampone et al., 2008) for the spinel facies equilibration in non-reacted peridotites.

The reactive melt percolation in the spinel lherzolite column leads to the progressive replacement of mantle pyroxenes by olivine, and thus to the formation of a dunite (Fig. 11). During progressive reaction, the porosity in the rock column increases from 1% in the starting lherzolite to 3% in the replacive dunite, as expected in a melt-rock reaction process characterized by $[M_a/M_c] > 1$. The modified melt composition, i.e. the melt in equilibrium with the spinel dunite (Fig. 11b, Table S8), shows global REE enrichment at constant LREE fractionation, and olivine in equilibrium with the modified melt (Yb_N = 0.35 times C1, Dy_N/Yb_N = 0.31, Fig. 11b) fit well the analyzed HREE patterns of olivines in the spinel dunite (Fig. 11b), both in terms of absolute concentration (Yb_N = 0.3–0.38 times C1) and fractionation (Dy_N/Yb_N = 0.26–0.43). We thus infer that the enriched REE compositions measured in olivines from the spinel dunite are acquired by equilibration of the olivine matrix with the percolating melt, modified after reactive porous flow in the spinel peridotites.

Olivines from the South Lanzo replacive dunites documented by Sanfilippo et al. (2014, 2017) show lower absolute trace element contents (Yb_N = 0.21–0.31 times C1; Ti = 26–33 ppm) than olivines in spinel dunites from the Mt. Maggiore (this study; Yb_N = 0.3–0.38 times C1). However, Sanfilippo et al. (2014, 2017) interpreted these elongated replacive dunite bodies, more than decametre-size, as dunite channels allowing focussed flow of a MORB-type melt. They considered the lack of a "reactive signature" of incompatible trace elements in olivines of Lanzo replacive dunites as reflecting equilibration with melts migrating through them by channelized flow, at high melt/rock ratios (Kelemen et al., 1995b; Spiegelman and Kelemen, 2003). In the Mt. Maggiore peridotites, the studied dunites are found as metre-size dunitic pods, and not as the elongated bodies commonly ascribed to channelized flow at high melt/rock ratios (Kelemen et al., 1995a). We infer that dunite formation involved moderate melt/rock ratios (<20–40%; Rosenberg and Handy, 2005; consistent with the preservation of clear olivine CPOs described above), which did not allow the formation of high-porosity dunite channels. The REE-enriched patterns analyzed in olivines from the Mt. Maggiore spinel dunites (Fig. 11b) thus represent the preserved "reactive signature" of incompatible elements, as a consequence of melt/rock ratios involved in the reactive porous flow lower than those required to form high-porosity dunite channels (Kelemen et al., 1995b; Sanfilippo et al., 2017).

9.2. Origin of hybrid troctolites by plagioclase-facies melt impregnation

At Mt. Maggiore, spinel peridotites (including clinopyroxene-poor spinel lherzolites, reacted harzburgites and dunites) grade to plagioclase-bearing lithotypes across the impregnation front observed at kilometre-scale in the field (Figs. 1, 3) (Piccardo and Guarnieri, 2010; Rampone et al., 2008). The plagioclase peridotites show microstructures indicative of an olivine-dissolving, [plagioclase + orthopyroxene]-crystallizing melt-rock interaction. In the studied area, the plagioclase peridotites are in contact with metre-size troctolitic bodies showing variable modal composition, from 70% to 90% of olivine (Fig. 5, Table 1) and up to 30% of interstitial minerals (plagioclase ± clinopyroxene). These olivine-rich troctolites and troctolites show similar microstructures to the plagioclase peridotites, indicative of an olivine-dissolving, plagioclase-crystallizing melt-rock interaction. Olivine-rich troctolites and troctolites also show large variations in trace element (Yb, Ti, Y, Zr) contents and HREE fractionation of olivine (Figs. 8, 9, 10), at almost constant Fo = 89.4–90.2, difficult to reconcile with a simple "cumulate" origin (Piccardo and Guarnieri, 2010; Rampone et al., 1997; Sanfilippo et al., 2014). The direct association between spinel peridotites and dunites grading to plagioclase peridotites and troctolites, respectively, through the impregnation front, the melt-rock reaction microstructures and trace elements compositional variability analyzed in the troctolites thus support a replacive origin of the troctolitic bodies. Their formation is likely related to the impregnation of pristine spinel dunites and dissolution of up to 30% of the pre-existing olivine matrix (Table 1).

In the following, we discuss the textural and microstructural evolution of the olivine matrix during impregnation of the spinel dunite and replacive formation of olivine-rich troctolite and troctolite. We then discuss the depleted and SiO_2-rich chemical signature of impregnating melts and provide a REE modelling of the melt impregnation process, to account for the observed mineral compositions in the troctolites.

9.2.1. Structural evolution during impregnation

Textural variations related to dissolution-precipitation reactions and replacive formation of olivine-rich troctolites have been extensively described in oceanic settings (Drouin et al., 2010; Ferrando et al., in press), ophiolites (Rampone et al., 2016; Sanfilippo et al., 2013) and melt-rock interaction experimental studies (Van den Bleeken et al., 2011; Saper and Liang, 2014). The described hybrid troctolites are characterized by rounded grains of olivines, enclosed in poikilitic minerals crystallized from the percolating melt. Similar crystallographic orientations of neighbouring rounded olivine grains suggest that they formerly belonged to a single olivine grain, corroded and disrupted by the reactive melt (Drouin et al., 2010; Suhr et al., 2008). In this study, the

field-controlled geological setting enables the direct observation of the evolution of textures from the dunitic protolith to the troctolitic end-product during progressive impregnation process (i.e., at decreasing modal contents of olivine). Olivines in the dunite are deformed, irregular and very coarse grained, up to 3 cm in size (Figs. 4, 5, 6). Olivine corrosion in the dunite starts at triple grain junctions (Fig. 4a) and evolves following grain boundaries (Fig. 4b), while crystallizing interstitial plagioclase. In the most impregnated samples, the extensive corrosion of olivine leads to the disruption of large irregular olivines into several smaller and rounded olivine grains (Fig. 4c,d) that are enclosed in the poikilitic plagioclase. Disrupted olivines often show less deformation than the former dunitic olivine (Fig. 5), suggesting a preferential corrosion along subgrain boundaries, as previously inferred by Suhr et al. (2008) and Drouin et al. (2010) in the Mid-Atlantic Ridge olivine-rich troctolites.

The quantification of the textural evolution of the olivine matrix from spinel dunite to troctolite reveals a correlation between the modal composition of olivine and the calculated mean grain number, grain area, aspect ratio and shape factor (Fig. 6). During progressive impregnation of the dunite (i.e. decreasing modal olivine), we observe an increase in grain number (from 12 to 59), accompanied with a decrease in grain area (from 38.8 mm^2 to 4.6 mm^2), aspect ratio (from 1.85 to 1.43), shape factor (from 2.49 to 1.77) and PARIS factor (from 179% to 105%) of olivine grains (Fig. 6). This evolution is indicative of the progressive corrosion and disruption of the dunitic matrix by the reactive melt (Fig. 5) (Drouin et al., 2010). The end-product of the impregnation process is a troctolite, composed of up to 30% of interstitial minerals, characterized by undeformed small rounded olivine grains enclosed in poikilitic plagioclase and clinopyroxene (Figs. 4, 5, 6). The decreasing concentration of misorientation along [010] olivine axis, together with a decrease in Grain Orientation Spread (GOS from 3.61 to 2.71) from dunite to olivine-rich troctolite to troctolite (Fig. 7c,e,f) is consistent with the described process of preferential corrosion along subgrain boundaries, and the decrease in grain deformation during reaction and disruption of a coarse deformed olivine into several rounded smaller olivines (Drouin et al., 2010; Suhr et al., 2008). Our EBSD analyses demonstrate the whole textural evolution, from the mantle protolith to the troctolite end-product, previously inferred to explain the origin of olivine-rich troctolites in oceanic and ophiolitic settings (Drouin et al., 2010; Rampone et al., 2016; Sanfilippo et al., 2013; Suhr et al., 2008). Magmatic cumulate textures in olivine-rich troctolites and troctolites can thus develop as a consequence of dissolution-precipitation reactions in a mantle-derived protolith.

No major change of olivine CPO is observed during impregnation and replacive formation of plagioclase peridotites and hybrid troctolites. Olivines in the plagioclase peridotite show an axial-[100] CPO, and olivines in the troctolite show an axial-[010] CPO, similar to the spinel lherzolite and spinel dunite protolith, respectively (Fig. 7). The preservation of the protolith CPO of olivine in plagioclase peridotite and troctolite, suggests low instantaneous melt-rock ratios involved in the impregnation process (Higgie and Tommasi, 2012). Our results differ from the olivine CPO randomization described during the replacive formation of olivine-rich troctolites from the Atlantis Massif (Drouin et al., 2010), suggesting melt/rock ratios allowing for the loss of cohesion of the solid matrix. The latter is consistent with the higher melt supplies required to build the gabbroic sequence in which the olivine-rich troctolites are included at the Mid-Atlantic Ridge (Drouin et al., 2009, 2010; Ferrando et al., in press). Overall, this structural evolution indicates that there is no universal CPO signature of melt-rock interactions originating hybrid troctolites (Drouin et al., 2010), since the modification or preservation of the protolith CPO of olivine entirely depends on the physical parameters (melt/rock ratio, temperature, pressure, strain, water content; Karato et al., 2008; Jung et al., 2009) involved in each melt-rock reaction stage.

9.2.2. Chemical signature of impregnating melts

Despite being part of the same impregnation event crystallizing plagioclase + orthopyroxene in the plagioclase peridotite, no interstitial orthopyroxene is found in the troctolites. Numerous studies describe the impregnation of peridotites by a silica-saturated melt, leading to

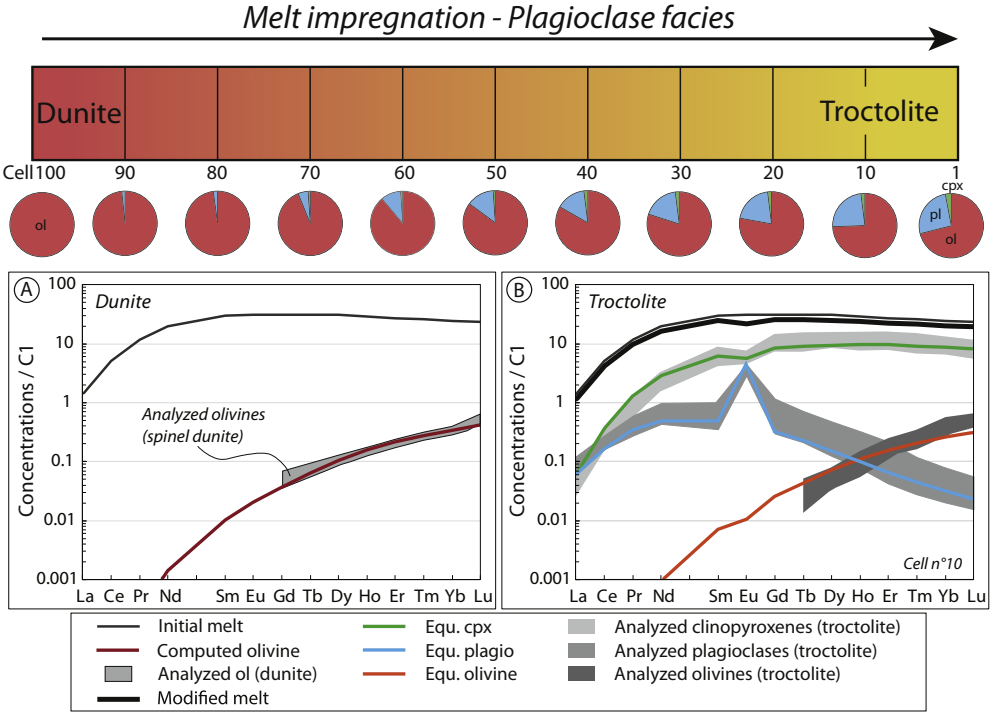

Fig. 12. Evolution of chondrite-normalized REE abundances and modal compositions computed by numerical simulation (Plate model, Vernières et al., 1997) during a process of impregnation at plagioclase facies. Detail of input parameters is given in the text. C1-chondrite normalization values after Sun and McDonough (1989). A: initial stage, spinel dunite; B: troctolite formed after melt impregnation.

the crystallization of plagioclase + orthopyroxene (Dijkstra et al., 2003; Dygert et al., 2016; Piccardo et al., 2007; Rampone et al., 2008; Rampone and Borghini, 2008; Van den Bleeken et al., 2011). They suggest that the impregnating melt acquired its silica-rich, orthopyroxene-saturated signature during a previous pyroxene-dissolving, olivine-crystallizing reactive porous flow in the spinel facies (Rampone et al., 2008). Kelemen et al. (1995b) and Dijkstra et al. (2003) showed that melt fractions produced by shallow mantle melting underneath mid-ocean ridges have more SiO_2-rich compositions than high-pressure mantle melts and are thus closer to orthopyroxene saturation (Dijkstra et al., 2003). The reaction of these melts with the host harzburgitic wall-rock, dissolving pyroxenes and crystallizing olivine, will rapidly drive the melt to orthopyroxene-saturation (Dijkstra et al., 2003; Kelemen et al., 1995b). However, the absence of interstitial orthopyroxene crystallization in the dunites and troctolites suggests that the orthopyroxene saturation of impregnating melts observed in the plagioclase peridotite is not only related to the spinel-facies reactive melt percolation. Rather, saturation is reached only during shallower dissolution-precipitation reactions involving pyroxene corrosion during impregnation. Microstructures characterizing the impregnation stage indicate the corrosion of olivine + mantle pyroxenes in the plagioclase peridotites (Piccardo and Guarnieri, 2010; Rampone et al., 2008), whereas only olivine is being corroded during impregnation of the spinel dunite. Therefore, we infer that the difference in the melt-rock interaction occurring in peridotites and dunites (peridotite-dissolution vs olivine-dissolution, respectively) leads to local variations in the melt compositions, resulting in orthopyroxene saturation in the melt percolating the peridotites (Dijkstra et al., 2003).

Previous studies of the Mt. Maggiore plagioclase peridotites and troctolites interpreted the impregnating melts to be previously modified by the spinel facies reactive porous flow (Rampone et al., 1997, 2008). They reported geochemical compositions of interstitial minerals (clinopyroxene and plagioclase) in equilibrium with a LREE depleted, M-HREE-enriched melt (Piccardo and Guarnieri, 2010; Rampone et al., 1997, 2008). The M-HREE enrichment was thought to be acquired during pyroxene-dissolving, olivine-crystallizing reactive melt percolation (AFC modelling, Rampone et al., 2008). Our Plate Model numerical simulation of the dunitization stage (see Discussion above) confirms the M-HREE-enriched signature of the melt modified after the spinel facies melt-rock interaction.

In order to explain the REE compositional variations documented in interstitial minerals in the troctolite (Fig. 9c,e), as well as the observed change in HREE fractionation between olivines in the dunite ($Dy_N/Yb_N = 0.26–0.43$) and in the troctolite ($Dy_N/Yb_N = 0.10–0.19$) (Fig. 9b), we performed a second step of Plate Model simulation of the impregnation process in the spinel dunites (Fig. 12a). The selected host rock and input melt composition are the output of the first stage of reactive melt percolation, namely a spinel dunite (100% olivine, 3% porosity, $Yb_N = 0.35$ times C1, $Dy_N/Yb_N = 0.31$) impregnated by a LREE-depleted, M-HREE-enriched melt, modified during the spinel-facies reactive percolation (Table S7). We assumed the following reaction:

$$\text{olivine}_2 + \text{melt}_2 = 0.9\ \text{plag} + 0.1\ \text{cpx} + \text{melt}_3$$

in which olivine ($M_a = 100\%$ olivine) is dissolved by the impregnating melt ($melt_2$), while crystallizing interstitial plagioclase and clinopyroxene ($M_c = 90\%$ plagio + 10% cpx), at global [$M_a/M_c = 0.96$]. Partition coefficients used for olivine and clinopyroxene were the same as those used for the spinel facies reactive percolation stage (Table S8). For plagioclase, we used a selected compilation of partition coefficients from Bédard (2001); Aigner-Torres et al. (2007) and Laubier et al. (2014) (Table S8).

Plate Model results show that the impregnation of the spinel dunite progressively leads to the dissolution of olivine and to the crystallization of plagioclase and clinopyroxene, thus causing the replacive formation of a hybrid troctolite composed of Ol:Plag:Cpx = 0.73:0.25:0.02 (Fig. 12b), similar to what is observed in the field (Table 1). The porosity decreases during impregnation, from 3% in the spinel dunite to 2% in the troctolite, as expected from a process characterized by a [M_a/M_c] < 1. The modified melt composition, i.e. in equilibrium with the replacive troctolite, preserves its LREE depletion and is slightly less enriched in M-HREE (up to 28 times C1, Table S8) with respect to the input melt (Fig. 12b). A remarkable feature is the development of a negative Eu anomaly in the modified melt composition after crystallization of plagioclase.

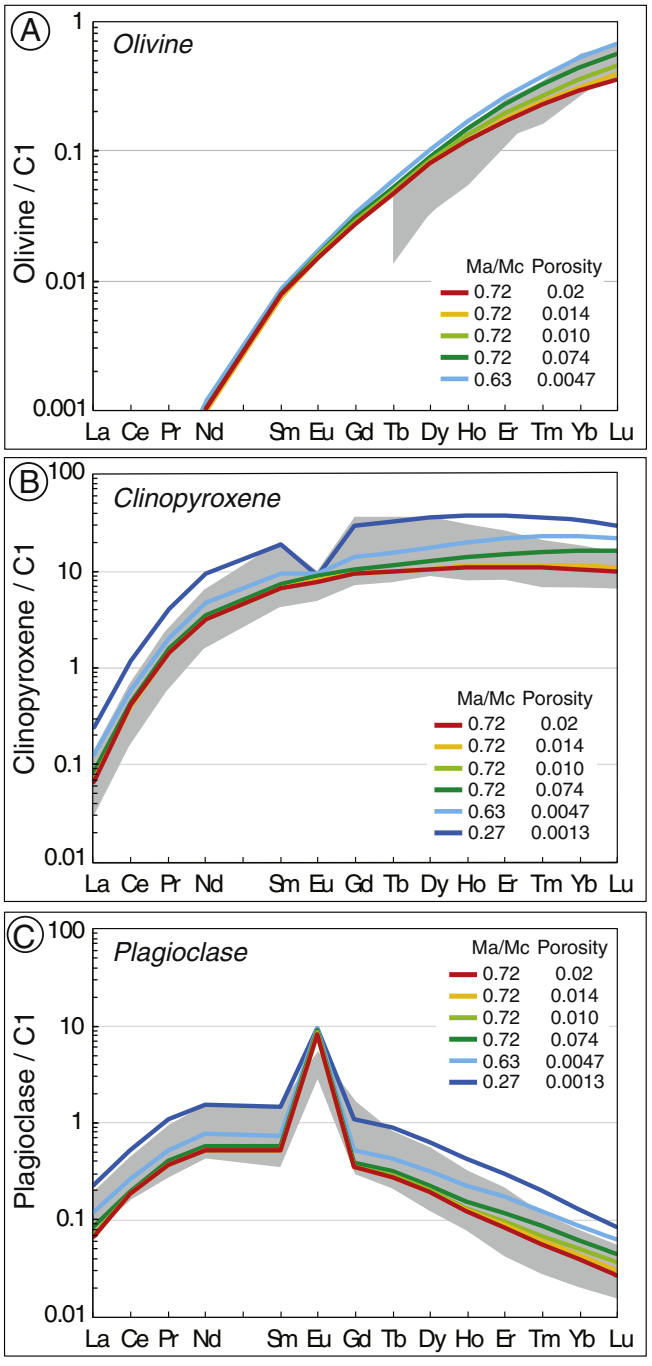

Fig. 13. Evolution of chondrite-normalized REE abundances of rock-forming minerals by numerical simulation (Plate Model, Vernières et al., 1997) during last steps of impregnation at decreasing melt mass and closure of porosity. Detail of input parameters is given in the text. C1-chondrite normalization values after Sun and McDonough (1989). A: olivine; B: Clinopyroxene; C: Plagioclase.

Plagioclase in equilibrium with the modified melt fit well the analyzed compositions of plagioclase cores in the troctolites, both in terms of LREE fractionation and absolute REE concentrations (Fig. 12b). It is remarkable, however, that plagioclase REE contents display large variations at constant LREE fractionation both between different lithotypes and within single grains (e.g. cores of large crystals vs. thin interstitial rims). Specifically, the progressive decrease in interstitial plagioclase modal content from troctolite to olivine-rich troctolite is correlated with an enrichment in plagioclase trace elements absolute concentrations (Sm_N up to 1.5 times C1) (Figs. 9, 10). As for plagioclase, computed clinopyroxene in equilibrium with the modified melt fit well the analyzed compositions of clinopyroxene cores in the troctolite. However, we observed significant REE enrichments at the rims of large clinopyroxene crystals, as well as in thin interstitial grains (Figs. 9, 10), similar to what was described in previous papers (Piccardo and Guarnieri, 2010; Rampone et al., 1997, 2008). In these studies, within-grain variations in interstitial minerals (plagioclase and clinopyroxene) were interpreted as the effect of late-stage crystallization of trapped melt fractions.

Computed olivine in equilibrium with the troctolite-forming melt shows lower HREE absolute concentrations and MREE/HREE fractionation ($Yb_N = 0.29$ times C1, $Dy_N/Yb_N = 0.3$) than olivines analyzed in the troctolite ($Yb_N = 0.26$–0.59 times C1, $Dy_N/Yb_N = 0.10$–0.19) (Fig. 12b). This discrepancy cannot be explained by a subsolidus reequilibration between clinopyroxene and olivine (Sun and Liang, 2014), since most of the troctolites are composed exclusively of olivine + interstitial plagioclase (Fig. 5; Table 1). Moreover, subsolidus reequilibration with clinopyroxene would lower HREE absolute contents of olivine (Sun and Liang, 2014), as observed in spinel peridotite (see Discussion above), whereas HREE contents of olivine in the troctolites are higher than the computed olivine in equilibrium with the impregnating melt (Fig. 12b). This is further supported by high equilibration temperatures (1150 °C and 1250 °C) computed using olivine-clinopyroxene HREE partitioning in troctolite (Sun and Liang, 2012, 2013a, b, 2014) (Fig. S3), consistent with previous geothermometric estimates of the impregnation stage reported by Rampone et al. (2008).

In order to explain the REE enrichments in interstitial plagioclase and clinopyroxene as well as the stronger MREE/HREE fractionation in olivine of troctolites, we have modelled further crystallization steps at decreasing melt mass, resulting in the closure of the porosity (Fig. 13). The $[M_a/M_c]$ ratio varies along the reaction process from 0.72 to 0.27 for the final crystallization step. During the progressive crystallization and decrease in porosity (from 2% to 0.47%), the melt composition evolves towards a fractionated HREE-enriched composition. Olivines in equilibrium with this HREE-enriched melt ($Yb_N = 0.54$ times C1; $Dy_N/Yb_N = 0.2$) fit the analyzed MREE-HREE concentrations of olivine in the troctolites ($Yb_N = 0.26$–0.59 times C1, $Dy_N/Yb_N = 0.10$–0.19) (Fig. 13a).

During the last increments of crystallization (from 0.47% to 0.13% porosity), the melt shows a global REE enrichment, while preserving its LREE fractionation (Fig. 13b,c). Plagioclase and clinopyroxene in equilibrium with the progressively REE-enriching melt cover the range of variation analyzed in crystal cores and rims of the plagioclase peridotite, olivine-rich troctolite and troctolite, both in terms of absolute REE concentrations and LREE fractionation (Fig. 13b,c). The modelled process of impregnation at decreasing melt mass (from 2% to 0.13% porosity) is consistent with the process of trapped melt crystallization previously proposed by Rampone et al. (1997, 2008) and Piccardo and Guarnieri (2010) to explain the trace elements (Ti, Zr, Y, REE) enrichments analyzed at the rims of large clinopyroxene crystals (Figs. 9, 10). The correlation between the plagioclase absolute REE concentrations and modal content of olivine (REE enrichments at higher

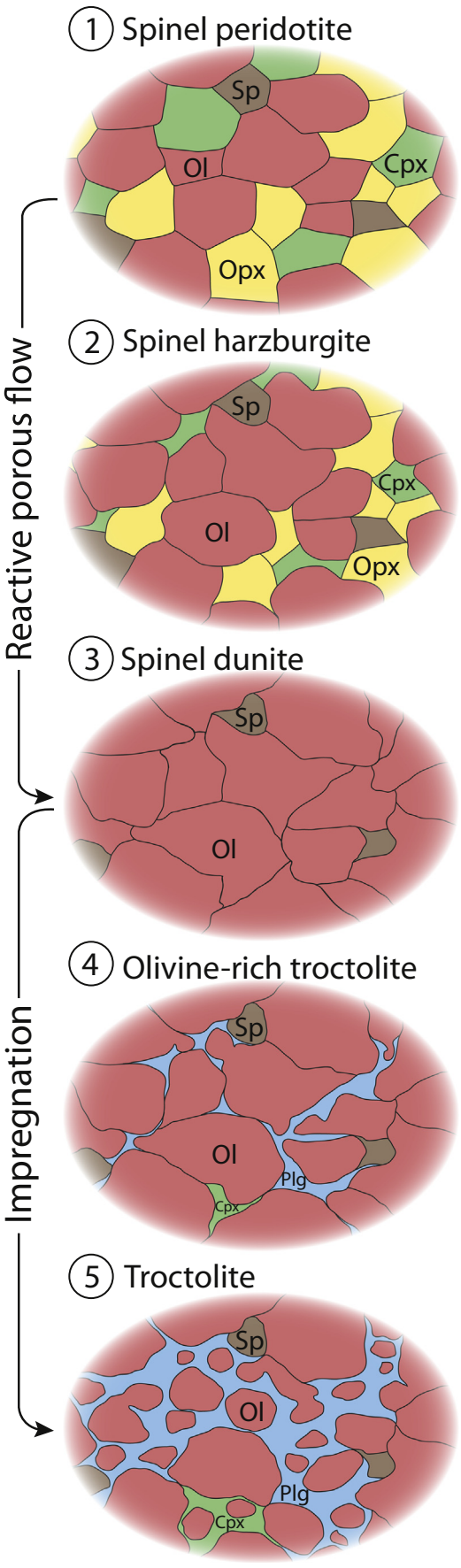

Fig. 14. Representative sketch of the textural evolution from spinel lherzolite to troctolite during multi-stage melt-rock interaction history.

modal content of olivine) is indicative of an increased contribution of trapped melt crystallization in olivine-rich zones, and thus of lower instantaneous melt/rock ratios during their impregnation.

10. Summary and concluding remarks

The Mt. Maggiore peridotitic body is an ideal case study to investigate the field-controlled evolution from spinel lherzolite to spinel dunite to hybrid troctolite (Fig. 14), after two distinct melt-rock interaction processes. The first melt-rock interaction is an olivine-crystallizing pyroxene-dissolving reactive percolation of a LREE-depleted melt, ultimately resulting in the formation of replacive dunite at spinel facies. This stage led to: (1) olivine growth at the expense of mantle pyroxenes, and development of very coarse and irregular texture of the olivine matrix in the spinel dunite, (2) structural changes of olivine CPO from axial-[100] in the spinel lherzolite to axial-[010] in the replacive dunite, (3) REE enrichment in the olivine matrix during progressive dunitization.

At shallower plagioclase facies, the melt impregnation of the spinel lherzolites and dunites caused the replacive formation of plagioclase peridotites and hybrid troctolites, respectively. This olivine-dissolving, [plagioclase + clinopyroxene]-crystallizing melt-rock interaction is documented in the troctolites by: (1) partial dissolution and disruption of the dunitic olivine matrix by low instantaneous melt/rock ratios, leading to a textural evolution towards small rounded undeformed olivine grains enclosed in poikilitic plagioclase, (2) preservation of the olivine CPO from the spinel-facies protoliths, (3) crystallization of LREE-depleted, HREE-enriched interstitial clinopyroxene and plagioclase from the melt modified after reactive melt percolation, and change of the MREE-HREE fractionation in the olivine matrix, and (4) REE enrichments in clinopyroxene rims and interstitial plagioclase during late-stage trapped melt crystallization.

The field-controlled study of the evolution from spinel lherzolite protolith to the troctolite end-product points to the possible CPO and geochemical inheritance from the protolith during processes of melt-rock interaction (depending on the involved melt-rock ratio). As a result, the structural and geochemical features analyzed in hybrid lithotypes are representative not only of the last event of melt-rock interaction, but of the whole evolution from mantle protolith to hybrid end-product. Olivine is the only mineral present in all lithotypes during the evolution from mantle lherzolites to replacive dunites to hybrid troctolites, therefore trace elements analyses in olivine are a perfect tool to investigate these melt-rock interaction processes and a good understanding of trace elements behaviour in olivine is of upmost importance.

Supplementary data to this article can be found online at https://doi.org/10.1016/j.lithos.2018.02.025.5

Acknowledgements

We thank Dr. Hidas, K. and Prof. Tribuzio, R. for their positive feedback and improvement of the quality of the paper. We would like to thank Paolo Campanella and Alessandra Gavoglio, as well as Christophe Nevado and Doriane Delmas for the realisation of the thin section and the high-quality polishing. We also thank Fabrice Barou for assistance with the EBSD analyses, Andrea Risplendente for assistance with the EPMA analyses, and Vincent Faucheux for assistance with field work. This project has been supported by the People Programme (Marie Curie Actions) of the European Union's Seventh Framework Programme FP7/2007–2013/under REA-Grant Agreement No. 608001, 'ABYSS'.

References

Aigner-Torres, M., Blundy, J., Ulmer, P., Pettke, T., 2007. Laser ablation ICPMS study of trace element partitioning between plagioclase and basaltic melts: an experimental approach. Contributions to Mineralogy and Petrology 153:647–667. https://doi.org/10.1007/s00410-006-0168-2.

Bédard, J.H., 2001. Parental magmas of the Nain plutonic suite anorthosites and mafic cumulates: a trace element modelling approach. Contributions to Mineralogy and Petrology 141:747–771. https://doi.org/10.1007/s004100100268.

Ben Ismail, W., Mainprice, D., 1998. An olivine fabric database: an overview of upper mantle fabrics and seismic anisotropy. Tectonophysics 296:145–157. https://doi.org/10.1016/S0040-1951(98)00141-3.

Ben Ismail, W., Barruol, G., Mainprice, D., 2001. The Kaapvaal craton seismic anisotropy: petrophysical analyses of upper mantle kimberlite nodules. Geophysical Research Letters 28:2497–2500. https://doi.org/10.1029/2000GL012419.

Borghini, G., Rampone, E., Crispini, L., De Ferrari, R., Godard, M., 2007. Origin and emplacement of ultramafic-mafic intrusions in the Erro-Tobbio mantle peridotite (Ligurian Alps, Italy). Lithos 94:210–229. https://doi.org/10.1016/j.lithos.2006.06.014.

Boudier, F., 1991. Olivine xenocrysts in picritic magmas: an experimental and microstructural study. Contributions to Mineralogy and Petrology 109, 114–123.

Bunge, H.J., 1982. Texture Analysis in Material Sciences. Butterworths, London.

Carter, N.L., Avé Lallemant, H.G., 1970. High temperature deformation of dunite andperidotite. Geological Society of America Bulletin 81, 2181–2202.

Collier, M.L., Kelemen, P.B., 2010. The case for reactive crystallization at Mid-Ocean ridges. Journal of Petrology 51:1913–1940. https://doi.org/10.1093/petrology/egq043.

Coumans, J.P., Stix, J., Clague, D.A., Minarik, W.G., Layne, G.D., 2016. Melt-rock interaction near the Moho: evidence from crystal cargo in lavas from near-ridge seamounts. Geochimica et Cosmochimica Acta 191:139–164. https://doi.org/10.1016/j.gca.2016.07.017.

D'Errico, M.E., Warren, J.M., Godard, M., 2016. Evidence for chemically heterogeneous Arctic mantle beneath the Gakkel ridge. Geochimica et Cosmochimica Acta 174: 291–312. https://doi.org/10.1016/j.gca.2015.11.017.

De Hoog, J.C.M., Gall, L., Cornell, D.H., 2010. Trace-element geochemistry of mantle olivine and application to mantle petrogenesis and geothermobarometry. Chemical Geology 270:196–215. https://doi.org/10.1016/j.chemgeo.2009.11.017.

Dick, H.J.B., Tivey, M.A., Tucholke, B.E., 2008. Plutonic foundation of a slow-spreading ridge segment: oceanic core complex at Kane Megamullion, 23°30′N, 45°20′W. Geochemistry, Geophysics, Geosystems 9, Q05014. https://doi.org/10.1029/2007GC001645.

Dick, H.J.B., Lissenberg, C.J., Warren, J.M., 2010. Mantle melting, melt transport, and delivery beneath a slow-spreading ridge: the paleo-MAR from 23°15′N to 23°45′N. Journal of Petrology 51:425–467. https://doi.org/10.1093/petrology/egp088.

Dijkstra, A.H., Drury, M.R., Vissers, R.L.M., 2001. Structural petrology of plagioclase peridotites in the West Othris Mountains (Greece): melt impregnation in mantle lithosphere. Journal of Petrology 42:5–24. https://doi.org/10.1093/petrology/42.1.5.

Dijkstra, A.H., Barth, M.G., Drury, M.R., Mason, P.R.D., Vissers, R.L.M., 2003. Diffuse porous melt flow and melt-rock reaction in the mantle lithosphere at a slow-spreading ridge: a structural petrology and LA-ICP-MS study of the Othris peridotite massif (Greece). Geochemistry, Geophysics, Geosystems 4:8613. https://doi.org/10.1029/2001GC000278.

Drouin, M., Godard, M., Ildefonse, B., Bruguier, O., Garrido, C.J., 2009. Geochemical and petrographic evidence for magmatic impregnation in the oceanic lithosphere at Atlantis Massif, Mid-Atlantic Ridge (IODP hole U1309D, 30°N). Chemical Geology 264:71–88. https://doi.org/10.1016/j.chemgeo.2009.02.013.

Drouin, M., Ildefonse, B., Godard, M., 2010. A microstructural imprint of melt impregnation in slow spreading lithosphere: olivine-rich troctolites from the Atlantis Massif, Mid-Atlantic Ridge, 30°N, IODP hole U1309D. Geochemistry, Geophysics, Geosystems 11, Q06003. https://doi.org/10.1029/2009GC002995.

Dygert, N., Liang, Y., Kelemen, P.B., 2016. Formation of plagioclase lherzolite and associated Dunite-Harzburgite-Lherzolite sequences by multiple episodes of melt percolation and melt-rock reaction: an example from the Trinity ophiolite, California, USA. Journal of Petrology 57:815–838. https://doi.org/10.1093/petrology/egw018.

Ferrando, C., Godard, M., Ildefonse, B., Rampone, E., 2018. Melt transport and mantle assimilation at Atlantis Massif (IODP site U1309): evidence from chemical profiles along olivine crystallographic axes. Lithos https://doi.org/10.1016/j.lithos.2018.01.012 (this volume, in press).

Foley, S.F., Prelevic, D., Rehfeldt, T., Jacob, D.E., 2013. Minor and trace elements in olivines as probes into early igneous and mantle melting processes. Earth and Planetary Science Letters 363:181–191. https://doi.org/10.1016/j.epsl.2012.11.025.

Heilbronner, R., Tullis, J., 2002. The effect of static annealing on microstructures and crystallographic preferred orientations of quartzites experimentally deformed in axial compression and shear. Geological Society of London, Special Publication 200, 191–218.

Higgie, K., Tommasi, A., 2012. Feedbacks between deformation and melt distribution in the crust-mantle transition zone of the Oman ophiolite. Earth and Planetary Science Letters 359–360:61–72. https://doi.org/10.1016/j.epsl.2012.10.003.

Higgie, K., Tommasi, A., 2014. Deformation in a partially molten mantle: constraints from plagioclase lherzolites from Lanzo, western Alps. Tectonophysics 615–616:167–181. https://doi.org/10.1016/j.tecto.2014.01.007.

Holtzman, B.K., Kohlstedt, D.L., Zimmerman, M.E., Heidelbach, F., Hiraga, T., Hustoft, J., 2003. Melt segregation and strain partitioning: implications for seismic anisotropy and mantle flow. Science 301:1227–1230. https://doi.org/10.1126/science.1087132.

Jackson, M.D., Ohnenstetter, M., 1981. Peridotite and gabbroic structures in the Monte Maggiore massif, alpine Corsica. Journal of Geology 89, 703–719 (doi: 0022-1376/81/8906-003).

Johnson, K.T.M., Dick, H.J.B., Shimizu, N., 1990. Melting in the oceanic upper mantle: an ion microprobe study of diopsides in abyssal peridotites. Journal of Geophysical Research 95:2661–2678. https://doi.org/10.1029/JB095iB03p02661.

Jung, H., Karato, S., 2001. Water-induced fabric transitions in olivine. Science 293: 1460–1463. https://doi.org/10.1126/science.1062235.

Jung, H., Mo, W., Green, H.W., 2009. Upper mantle seismic anisotropy resulting from pressure-induced slip transition in olivine. Nature Geoscience 2:73–77. https://doi.org/10.1038/NGEO389.

Kaczmarek, M.A., Tommasi, A., 2011. Anatomy of an extensional shear zone in the mantle, Lanzo massif, Italy. Geochemistry, Geophysics, Geosystems 12, Q0AG06. https://doi.org/10.1029/2011GC003627.

Karato, S., Jung, H., Katayama, I., Skemer, P., 2008. Geodynamic significance of seismic anisotropy of the upper mantle: new insights from laboratory studies. Annual Review of Earth and Planetary Sciences 36, 59–95 (doi: 0084-6597/08/0530-0059).

Kelemen, P.B., Shimizu, N., Salters, V.J.M., 1995a. Extraction of mid-ocean-ridge basalt from the upwelling mantle by focused flow of melt in dunite channels. Nature 375: 747–753. https://doi.org/10.1038/375747a0.

Kelemen, P.B., Whitehead, J.A., Aharonov, E., Jordahl, K.A., 1995b. Experiments on flow focusing in soluble porous media, with applications to melt extraction from the mantle. Journal of Geophysical Research 100:475–496. https://doi.org/10.1029/94JB02544.

Kelemen, P.B., Braun, M., Hirth, G., 2000. Spatial distribution of melt conduits in the mantle beneath oceanic spreading ridges: observations from the Ingalls and Oman ophiolites. Geochemistry, Geophysics, Geosystems 1. https://doi.org/10.1029/1999GC000012.

Kelemen, P.B., Kikawa, E., Miller, D.J., Shipboard Scientific Party, 2007. 1. Leg 209 summary: processes in a 20-km-thick conductive boundary layer beneath the Mid-Atlantic Ridge, 14°–16°N. Proceedings of the Ocean Drilling Program, Scientific Results vol. 209. Ocean Drilling Program, College Station TX:pp. 1–33. https://doi.org/10.2973/odp.proc.sr.209.001.2007.

Lambart, S., Laporte, D., Schiano, P., 2009. An experimental study of focused magma transport and basalt-peridotite interactions beneath mid-ocean ridges: implications for the generation of primitive MORB compositions. Contributions to Mineralogy and Petrology 157:429–451. https://doi.org/10.1007/s00410-008-0344-7.

Laubier, M., Grove, T.L., Langmuir, C.H., 2014. Trace element mineral/melt partitioning for basaltic and basaltic andesitic melts: an experimental and laser ICP-MS study with application to the oxidation state of mantle source regions. Earth and Planetary Science Letters 392:265–278. https://doi.org/10.1016/j.epsl.2014.01.053.

Le Roux, V., Tommasi, A., Vauchez, A., 2008. Feedback between melt percolation and deformation in an exhumed lithosphere-asthenosphere boundary. Earth and Planetary Science Letters 274:401–413. https://doi.org/10.1016/j.epsl.2008.07.053.

Liang, Y., Schiemenz, A., Hesse, M.A., Parmentier, E.M., 2011. Waves, channels, and the preservation of chemical heterogeneities during melt migration in the mantle. Geophysical Research Letters 38, L20308. https://doi.org/10.1029/2011GL049034.

Lissenberg, J.C., Dick, H.J.B., 2008. Melt-rock reaction in the lower oceanic crust and its implications for the genesis of mid-ocean ridge basalt. Earth and Planetary Science Letters 271:311–325. https://doi.org/10.1016/j.epsl.2008.04.023.

Lissenberg, C.J., MacLeod, C.J., Howard, K.A., Godard, M., 2013. Pervasive reactive melt migration through fast-spreading lower oceanic crust (Hess deep, equatorial Pacific Ocean). Earth and Planetary Science Letters 361:436–447. https://doi.org/10.1016/j.epsl.2012.11.012.

Mainprice, D., Tommasi, A., Couvy, H., Cordier, P., Frost, D.J., 2005. Pressure sensitivity of olivine slip systems and seismic anisotropy of Earth's upper mantle. Nature 433: 731–733. https://doi.org/10.1038/nature03266.

Mainprice, D., Bachmann, F., Hielscher, R., Schaeben, H., 2014. Descriptive tools for the analysis of texture projects with large datasets using MTEX: strength, symmetry and components. Geological Society of London, Special Publication 409. https://doi.org/10.1144/SP1409.1148.

Manatschal, G., Müntener, O., 2009. A type sequence across an ancient magma-poor ocean-continent transition: the example of the western alpine Tethys ophiolites. Tectonophysics 473:4–19. https://doi.org/10.1016/j.tecto.2008.07.021.

Marroni, M., Molli, G., Montanini, A., Tribuzio, R., 1998. The association of continental crust rocks with ophiolites in the northern Apennines (Italy): implications for the continent-ocean transition in the western Tethys. Tectonophysics 292:43–66. https://doi.org/10.1016/S0040-1951(98)00060-2.

Müntener, O., Piccardo, G.B., 2003. Melt migration in ophiolitic peridotites: the message from Alpine–Apennine peridotites and implications for embryonic ocean basin. In: Dilek, Y., Robinson, P.T. (Eds.), Ophiolites in Earth History: Geological Society of London Special Publication. 218, pp. 69–89 (doi: 0305-8719/03).

Müntener, O., Pettke, T., Desmurs, L., Meier, M., Schaltegger, U., 2004. Refertilization of mantle peridotite in embryonic ocean basins: trace element and Nd isotopic evidence and implications for crust-mantle relationships. Earth and Planetary Science Letters 221:293–308. https://doi.org/10.1016/S0012-821X(04)00073-1.

Paquet, M., Cannat, M., Brunelli, D., Hamelin, C., Humler, E., 2016. Effect of melt/mantle interactions on MORB chemistry at the easternmost southwest Indian ridge (61 to 67°E). Geochemistry, Geophysics, Geosystems 17:4605–4640. https://doi.org/10.1002/2016GC006385.

Piccardo, G.B., Müntener, O., Zanetti, A., Romairone, A., Bruzzone, S., Poggi, E., Spagnolo, A., 2004. The Lanzo south peridotite: melt/peridotite interaction in the mantle lithosphere of the Jurassic Ligurian Tethys. Ofioliti 29:37–62. https://doi.org/10.4454/ofioliti.v29i1.205.

Piccardo, G.B., Zanetti, A., Müntener, O., 2007. Melt/peridotite interaction in the southern Lanzo peridotite: field, textural and geochemical evidence. Lithos 94:181–209. https://doi.org/10.1016/j.lithos.2006.07.002.

Piccardo, G.B., Guarnieri, L., 2010. The Monte Maggiore peridotite (Corsica, France): a case study of mantle evolution in the Ligurian Tethys. Geological Society of London 337: 7–45. https://doi.org/10.1144/SP337.2 0305-8719/10.

Pirard, C., Hermann, J., O'Neill, H.S.T.C., 2013. Petrology and geochemistry of the crust-mantle boundary in a nascent arc, Massif du Sud ophiolite, New Caledonia, SW Pacific. Journal of Petrology 54:1759–1792. https://doi.org/10.1093/petrology/egt030.

Rampone, E., Piccardo, G.B., Vannucci, R., Bottazzi, P., 1997. Chemistry and origin of trapped melts in ophiolitic peridotites. Geochimica et Cosmochimica Acta 21, 4557–4569 (doi: 0016-7037/97).

Rampone, E., Piccardo, G.B., 2000. The ophiolite-oceanic lithosphere analogue: new insights from the Northern Apennines (Italy). In: Dilek, Y., Moores, E.M., Elthon, D., Nicolas, A. (Eds.), Ophiolites and Oceanic Crust: New Insights From Field Studies and the Oceanic Drilling Program. Geological Society of America Special Paper, Boulder 349:pp. 21–34. https://doi.org/10.1130/0-8137-2349-3.21.

Rampone, E., Borghini, G., 2008. Melt migration and intrusion in the Erro-Tobbio peridotites (Ligurian Alps, Italy): insights on magmatic processes in extending lithospheric mantle. European Journal of Mineralogy 20:573–585. https://doi.org/10.1127/0935-1221/2008/0020-1807.

Rampone, E., Romairone, A., Hofmann, A.W., 2004. Contrasting bulk and mineral chemistry in depleted mantle peridotites: evidence for reactive porous flow. Earth and Planetary Science Letters 2018:491–506. https://doi.org/10.1016/S0012-821X(03)00679-4.

Rampone, E., Piccardo, G.B., Hofmann, A.W., 2008. Multi-stage melt-rock interaction in the Mt. Maggiore (Corsica, France) ophiolitic peridotites: microstructural and geochemical evidence. Contributions to Mineralogy and Petrology 156:453–475. https://doi.org/10.1007/s00410-008-0296-y.

Rampone, E., Borghini, G., Godard, M., Ildefonse, B., Crispini, L., Fumagalli, P., 2016. Melt/rock reaction at oceanic peridotite/gabbro transition as revealed by trace element chemistry of olivine. Geochimica et Cosmochimica Acta 190:309–331. https://doi.org/10.1016/j.gca.2016.06.029.

Renna, M.R., Tribuzio, R., 2011. Olivine-rich troctolites from Ligurian ophiolites (Italy): evidence for impregnation of replacive mantle conduits by MORB-type melts. Journal of Petrology 52:1763–1790. https://doi.org/10.1093/petrology/egr029.

Renna, M.R., Tribuzio, R., Ottolini, L., 2016. New perspectives on the origin of olivine-rich troctolites and associated harrisites from the Ligurian ophiolites (Italy). Journal of the Geological Society 174. https://doi.org/10.1144/jgs2015-135.

Rosenberg, C.L., Handy, M.R., 2005. Experimental deformation of partially melted granite revisited: implications for the continental crust. Journal of Metamorphic Geology 23: 19–28. https://doi.org/10.1111/j.1525-1314.2005.00555.x.

Sanfilippo, A., Tribuzio, R., 2011. Melt transport and deformation history in a nonvolcanic ophiolitic section, northern Apennines, Italy: implications for crustal accretion at slow-spreading settings. Geochemistry, Geophysics, Geosystems 12, Q0AG04. https://doi.org/10.1029/2010GC003429.

Sanfilippo, A., Tribuzio, R., 2012. Building of the deepest crust at a fossil slow-spreading centre (Pineto gabbroic sequence, Alpine Jurassic ophiolites). Contributions to Mineralogy and Petrology 165:705–721. https://doi.org/10.1007/s00410-012-0831-8.

Sanfilippo, A., Dick, H.J.B., Ohara, Y., 2013. Melt-rock reaction in the mantle: mantle troctolites from the Parece Vela ancient back-arc spreading center. Journal of Petrology 54:861–885. https://doi.org/10.1093/petrology/egs089.

Sanfilippo, A., Tribuzio, R., Tiepolo, M., 2014. Mantle-crust interactions in the oceanic lithosphere: constraints from minor and trace elements in olivine. Geochimica et Cosmochimica Acta 141:423–439. https://doi.org/10.1016/j.gca.2014.06.012.

Sanfilippo, A., Morishita, T., Kumagai, H., Nakamura, K., Okino, K., Hara, K., Tamura, A., Arai, S., 2015. Hybrid troctolites from Mid-Ocean ridges: inherited mantle in the lower crust. Lithos 232:124–130. https://doi.org/10.1016/j.lithos.2015.06.025.

Sanfilippo, A., Dick, H.J.B., Ohara, Y., Tiepolo, M., 2016. New insights on the origin of troctolites from the breakaway area of the Godzilla Megamullion (Parece Vela back-arc basin): the role of melt-mantle interaction on the composition of the lower crust. Island Arc 25:220–234. https://doi.org/10.1111/iar.12137.

Sanfilippo, A., Tribuzio, R., Ottolini, L., Hamada, M., 2017. Water, lithium and trace element compositions of olivine from Lanzo South replacive mantle dunites (Western Alps): new constraints into melt migration processes at cold thermal regimes. Geochimica et Cosmochimica Acta 214:51–72. https://doi.org/10.1016/j.gca.2017.07.034.

Saper, L., Liang, Y., 2014. Formation of plagioclase-bearing peridotite and plagioclase-bearing wehrlite and gabbro suite through reactive crystallization: an experimental study. Contributions to Mineralogy and Petrology 167:985. https://doi.org/10.1007/s00410-014-0985-7.

Soustelle, V., Tommasi, A., Bodinier, J.L., Garrido, C.J., Vauchez, A., 2009. Deformation and reactive melt transport in the mantle lithosphere above a large-scale partial melting domain: the Ronda peridotite massif, southern Spain. Journal of Petrology 50: 1235–1266. https://doi.org/10.1093/petrology/egp032.

Soustelle, V., Tommasi, A., Demouchy, S., Ionov, D.A., 2010. Deformation and fluid-rock interaction in the supra-subduction mantle: microstructures and water contents in peridotite xenoliths from the Avacha volcano, Kamchatka. Journal of Petrology 51: 363–394. https://doi.org/10.1093/petrology/egp085.

Soustelle, V., Walte, N.P., Geeth, M.A., Manthilake, M., Frost, D.J., 2014. Melt migration and melt-rock reactions in the deforming Earth's upper mantle: experiments at high pressure and temperature. Geology 42:83–86. https://doi.org/10.1130/G34889.1.

Spiegelman, M., Kelemen, P.B., 2003. Extreme chemical variability as a consequence of channelized melt transport. Geochemistry, Geophysics, Geosystems 4:1055–1072. https://doi.org/10.1029/2002GC000336.

Suhr, G., Hellebrand, E., Johnson, K., Brunelli, D., 2008. Stacked gabbro units and intervening mantle: a detailed look at a section of IODP Leg 305, hole U1309D. Geochemistry, Geophysics, Geosystems 9, Q10007. https://doi.org/10.1029/2008GC002012.

Sun, S.S., McDonough, W.F., 1989. Chemical and isotopic systematics of oceanic basalts: implications for mantle composition and processes. Geological Society of London, Special Publication 42:313–345. https://doi.org/10.1144/GSL.SP.1989.042.01.19.

Sun, C., Liang, Y., 2012. Distribution of REE between clinopyroxene and basaltic melt along a mantle adiabat: effects of major element composition, water and temperature. Contributions to Mineralogy and Petrology 163:807–823. https://doi.org/10.1007/s00410-011-0700-x.

Sun, C., Liang, Y., 2013a. The importance of crystal chemistry on REE partitioning between mantle minerals (garnet, clinopyroxene, orthopyroxene, and olivine) and basaltic melts. Chemical Geology 358:23–36. https://doi.org/10.1016/j.chemgeo.2013.08.045.

Sun, C., Liang, Y., 2013b. Distribution of REE and HFSE between low-Ca pyroxene and lunar picritic glass melts around multiple saturation points. Geochimica et Cosmochimica Acta 119:340–358. https://doi.org/10.1016/j.gca.2013.05.036.

Sun, C., Liang, Y., 2014. An assessment of subsolidus re-equilibration on REE distribution among mantle minerals olivine, orthopyroxene, clinopyroxene, and garnet in peridotites. Chemical Geology 372:80–91. https://doi.org/10.1016/j.chemgeo.2014.02.014.

Tommasi, A., Tikoff, B., Vauchez, A., 1999. Upper mantle tectonics: three-dimensional deformation, olivine crystallographic fabrics and seismic properties. Earth and Planetary Science Letters 168:173–186. https://doi.org/10.1016/S0012-821X(99)00046-1.

Tommasi, A., Mainprice, D., Canova, G., Chastel, Y., 2000. Viscoplastic self-consistent and equilibrium-based modeling of olivine lattice preferred orientations: implications for the upper mantle seismic anisotropy. Journal of Geophysical Research 105: 7893–7908. https://doi.org/10.1029/1999JB900411.

Tommasi, A., Godard, M., Coromina, G., Dautria, J.M., Barsczus, H., 2004. Seismic anisotropy and compositionally induced velocity anomalies in the lithosphere above mantle plumes: a petrological and microstructural study of mantle xenoliths from French Polynesia. Earth and Planetary Science Letters 227:539–556. https://doi.org/10.1016/j.epsl.2004.09.019.

Tommasi, A., Vauchez, A., Ionov, D.A., 2008. Deformation, static recrystallization, and reactive melt transport in shallow subcontinental mantle xenoliths (Tok Cenozoic volcanic field, SE Siberia). Earth and Planetary Science Letters 272:65–77. https://doi.org/10.1016/j.epsl.2008.04.020.

Tommasi, A., Ishikawa, A., 2014. Microstructures, composition, and seismic properties of the Ontong Java Plateau mantle root. Geochemistry, Geophysics, Geosystems https://doi.org/10.1002/2014GC005452.

Tribuzio, R., Garzetti, F., Corfu, F., Tiepolo, M., Renna, M.R., 2016. U-Pb zircon geochronology of the Ligurian ophiolites (northern Apennine, Italy): implications for continental breakup to slow seafloor spreading. Tectonophysics 666:220–243. https://doi.org/10.1016/j.tecto.2015.10.024.

Tursack, E., Liang, Y., 2012. A comparative study of melt-rock reactions in the mantle: laboratory dissolution experiments and geological field observations. Contributions to Mineralogy and Petrology 163:861–876. https://doi.org/10.1007/s00410-011-0703-7.

Van den Bleeken, G., Müntener, O., Ulmer, P., 2011. Melt variability in percolated peridotite: an experimental study applied to reactive migration of tholeiitic basalt in the upper mantle. Contributions to Mineralogy and Petrology 161:921–945. https://doi.org/10.1007/s00410-010-0572-5.

Vernières, L., Godard, M., Bodinier, J.L., 1997. A plate model for the simulation of trace element fractionation during partial melting and magma transport in the Earth's upper mantle. Journal of Geophysical Research 102:24771–24784. https://doi.org/10.1029/97JB1946.

Warren, J.M., 2016. Global variations in abyssal peridotite compositions. Lithos 248-251: 193–219. https://doi.org/10.1016/j.lithos.2015.12.023.

Workman, R.K., Hart, S.R., 2005. Major and trace element composition of the depleted MORB mantle (DMM). Earth and Planetary Science Letters 231:53–72. https://doi.org/10.1016/j.epsl.2004.12.005.